

Andrew Anderson

•

Development of Cold-Wall Chemical Vapour Deposition Systems  
for the Growth of Carbon Nanotubes and Carbon Fibres

Andrew Ober Anderson

Submitted to Swansea University in fulfilment of the requirements for  
the Degree of Master of Science in  
Nanotechnology by Research

Swansea University

2020


Copyright: The Author, Andrew O. Anderson, 2023.

## Summary (Abstract)


This work investigates the construction of a cold wall chemical vapour deposition system for producing carbon nanotubes and carbon nanofibers from a solid carbon source, camphor. A high temperature ceramic heater was fabricated and utilized inside a 50 mm diameter quartz tube. This reaction takes place within an argon environment with no gas flow during the growth process. Ferrocene was used in the formation of iron nanoparticles on a zeolite substrate. The effects of reaction temperature on the produced carbon species were investigated using Raman spectroscopy and scanning electron microscopy. Carbon nanotubes as well as likely metal oxide nano-wires were successfully grown and identified using Raman spectroscopy and scanning electron microscopy. This work demonstrates that solid carbon sources can be used in a cold wall reactor designed to produce carbon nanomaterials. The reactor design is inexpensive and easy to construct with sufficient technical skills.

## Declarations and Statements

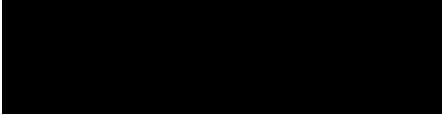
This work has not previously been accepted in substance for any degree and is not being concurrently submitted in candidature for any degree.

 Date 01/05/2020.....


This work is the result of my own independent study/investigation, except where otherwise stated. Other sources are acknowledged by footnotes giving explicit references. A bibliography is appended.

 Date 01/05/2020.....

I hereby give my consent for my work, if relevant and accepted, to be available for photocopying and for inter-library loan, and for the title and summary to be made available to outside organisations.

 Date 01/05/2020.....

Swansea Universities' ethical procedures were followed in this work.

 Date 01/05/2020.....

## Contents

Summary (Abstract) .....	2
Declarations and Statements.....	3
Contents.....	4
Acknowledgements.....	5
List of Tables and Figures.....	6
Definitions or Abbreviations .....	8
Chapter 1: Background .....	9
1.1 Properties .....	13
1.2 Growth Methods .....	16
1.3 Analytical techniques.....	19
Chapter 2: Reactor Construction .....	24
2.1 System Diagram and Schematics .....	24
2.2 Materials Selection .....	26
2.3 Growth Parameters .....	32
Chapter 3: Growth Protocol and Results .....	33
3.1 Growth Protocol .....	33
3.2 Results and Discussion.....	36
Chapter 4: Conclusions and Future Work.....	46
4.1 Conclusion and Discussion.....	46
Appendix A: Supplementary Data.....	48
Glossary.....	50
References .....	52

## Acknowledgements

I wish to show great appreciation to my advisor at Swansea University, Dr Alvin Orbaek White. He helped me to understand the right questions to ask. His fascination with understanding carbon nanotubes stirred a similar feeling in myself. His guidance also proved invaluable in helping me begin my literature review. I would also like to thank Dr Stuart Corr, my mentor in the United States. His belief in me inspired me to enrol in a graduate program. His invaluable input and experience helped me to manage my project and ensure this works timely completion. I would also like to thank Baylor College of Medicine and Swansea University for financial and material support that brought this project into reality. I would also like to thank my family and friends for continued support throughout my life.

## List of Tables and Figures

*Figure 1: (a) Carbon ring network inherent to all graphitic materials; a graphene sheet may be rolled into a tube with varying degrees of twist based on how the edges are connected known as chirality. The properties of the resulting tubes vary with chirality with armchair configuration tubes being metallic and well suited for conductive applications. [14] Bottom shows size comparison of tubular carbon structures with (b) being a SWCNT, (c) being a MWCNT, (d) being a carbon nanofibre, and (e) and (f) being carbon fibre.[13] ..... 11*

*Figure 2: Cross sectional view of (a) stacked cone CNF and (b) MWCNT. The graphitic planes of (a) stacked in a horizontal arrangement while in (b) they are vertically aligned..... 15*

*Figure 3: Diagram of CNT growth methods. (a) Arc discharge method. (b) Laser ablation method. (c) Chemical vapor deposition method ..... 16*

*Figure 4: Raman spectra comparison of CNTs (in blue) obtained via liquid injection reactor synthesis and commercially obtained CFs (FibreGlast L210530) (in orange). The  $I_d/I_g$  ratio is displayed on the graph in corresponding colours. Notice lack of peak around  $2700\text{ cm}^{-1}$  on CF spectra. This is the primary difference between the two spectra. All Raman spectra were obtained using 633 nm laser at 10% power with a 30 second acquisition time..... 21*

*Figure 5: Magnification equation and diagram relating focal length with objective diameter. .... 22*

*Figure 6: (a) SEM of as-grown LIR CNTs, (b) SEM of commercial CFs from an aligned sheet ..... 24*

*Figure 7: Electrical overview of the designed cold wall CVD system..... 26*

*Figure 8: Skeletal structure of camphor molecule. Camphor has a hexagonal carbon ring with a carbon atom splitting the middle, forming two pentagonal rings. Functional groups consist of three methyl and one ketone group. The aromatic carbon rings help in the formation of carbon ring free radicals that are the direct building blocks of CNTs. The oxygen atom may help prevent catalytic fouling by combining with amorphous carbon to form gaseous carbon oxides. .... 27*

*Figure 9 (a) 3D render of ceramic heater design (b) photographic overview of same..... 28*

*Figure 10: Ceramic heater temperature plot for sample 6. System displays oscillation possibly due to incorrect PID tuning. This temperature variation will increase the growth rate at higher temperatures [56] ..... 29*

*Figure 11: (a) Cold wall CVD reactor constructed in Houston, Texas (b) sSide view of heater assembly with labelled components (c) magnified photo of boxed region in image (a) showing side view of heater assembly ..... 30*

*Figure 12: Ferrocene molecule, consisting of central iron atom sandwiched between 2 cyclopentadienyl rings. High temperature decomposition yields iron nanoparticles that act as a catalyst for the CNT and CNF growth process. The size of iron nanoparticles is determined by ferrocene concentration, temperature of reaction, and time held at temperature. Diameter of catalyst particles determines whether CNT or CNF are grown as well as their resulting diameter. .... 31*

*Figure 13: EDS elemental analysis (performed on Hitachi desktop SEM) showing presence of iron (cyan), and silicon (green) confirming that ferrocene was decomposed into catalyst particles. Silicon is used to visualize zeolite as it is an aluminosilicate material. .... 33*

*Figure 14: (a) growth plate before heat application, (b) growth plate during heat application, (c) bell jar wired to growth plate post run, (d) growth plate with heater stage discoloration after many runs. (e)*

close up of growth plate sans heater post run. (f) close up of heater stage after first run. This visualizes a time lapse of the process. .... 36

Figure 15: *graph a, average spectra of samples grown at different temperatures. Control sample is CF. Sample spectra approaches CF spectra as temperature increases. Peaks indicate CF was grown. Graph b, average background intensity for each sample from 1400 cm<sup>-1</sup> to 1475 cm<sup>-1</sup>. This background is due to fluorescence within amorphous carbon. This shows a decrease in amorphous carbon as temperature increases. [59]* ..... 38

Figure 16: SEM of sample 2 grown at 600 °C. (a) No noticeable CNT or CF growth and (b) very little indication of iron catalyst structures. .... 40

Figure 17: SEM of sample 4, grown at 700 °C. (a) Multiple hair like filaments between zeolite cubes. (b) length of one of the longer fibres, this fibre also exhibits a 90° bend (c) CNTs also appear to be growing on zeolite faces. Small dot structures on surface of zeolite indicative of iron nanoparticle catalyst. .... 42

Figure 18: SEM of Sample 7 showing measurement of several different width CFs (a) zeolite faces appear covered in amorphous carbon as well as some tubular structures. (b) width measurement of one of the protruding fibres on the zeolite. (c) measurement of a wider structure on the zeolite. (d) 'pig-tail' like structure with width measurement. .... 44

Figure 19: SEM of sample 8 grown at 700 °C (a) showing formation of iron catalyst nanoparticles. (b) and (c) tubular networks on zeolite surface. (d) catalyst width measurements with error range..... 45

## Definitions or Abbreviations

$\mu\text{m}$  – micrometre

a.u. – arbitrary units

Ar – argon

BSE – backscattered electrons

$\text{C}_{60}$  – fullerene with 60 carbon atoms

CAD – computer aided design

CCD – charge coupled device; a type of sensor used to capture images digitally.

CF – carbon fibre

CNF – carbon nanofiber

CNT – carbon nanotube

CVD – chemical vapour deposition

DWCNT – double wall carbon nanotube

EDS – Energy-dispersive X-ray spectroscopy

ESRI – Energy Safety Research Institute

Hz – derived unit of frequency defined as one cycle per second

LIR – liquid injection reactor

MWCNT – multiwall carbon nanotube

NiCr – nickel chromium wire with high resistivity used a heating element

nm – nanometre

PID – proportional integral derivative control

scm – standard cubic centimetres per minute

SEM – scanning electron microscopy

SS – stainless steel

SWCNT – single wall carbon nanotube

Sweet  $\text{C}_{60}$  – Glycoconjugated  $\text{C}_{60}$

TEM – transmission electron microscopy

UV – ultra violet region of the electromagnetic spectrum

VGCF – vapour grown carbon fibre

Wt% -- ratio of substance in a mixture expressed as a percentage by weight



## Chapter 1: Background

Carbon is one of the most versatile elements in existence. Carbon has four valence electrons, whereby each may form a covalent bond with an adjacent atoms' valence electrons in pairs. Carbon is able to bond with itself repeatably in a series to form a chain. This process, known as catenation, is expressed as single, double, and triple covalent bonds between carbon atoms and leads to the many different allotropes of carbon including, graphite, diamond, amorphous carbon, and nanocarbons such as carbon nanotubes (CNTs), graphene, and Buckminsterfullerenes ( $C_{60}$ ). [1]  $C_{60}$  was first discovered in 1985 by Robert Curl, Harold Kroto, and Richard Smalley at Rice University in Houston, Texas, winning them the Nobel Prize in Chemistry in 1996. The  $C_{60}$  molecule is an allotrope of carbon that consists of spherical shell-shaped molecules composed of alternating pentyl and hexagonal carbon rings. This gives it the same shape and number of faces as a traditional football. Carbon has a diverse range of properties depending on the allotrope. Graphite is a very soft and optically opaque material that is often used in pencils to write on paper, while diamond is one of the hardest known substances and is highly transparent to visible light. Graphene is a 2D planar crystalline structure composed of carbon arranged in a hexagonal lattice. [2] Graphene was first fully isolated and characterized in 2004 by Andre Geim and Konstantin Novoselov at the University of Manchester, earning the duo the Nobel Prize in Physics in 2010. [3] Graphene is predicted to have the highest tensile strength of any known material at 130 GPa while structural steel has a tensile strength of 400 -550 MPa. [4] Graphite is composed of many layers of graphene in a stack. Single layer graphene is optically transparent due to high optical transmittance greater than 90% between 200 nm and 2500 nm wavelength of light. [5] [6] Graphite is opaque because light must pass through layer after layer of graphene until all the photons are absorbed. Another notable group of allotropes of carbon consists of 3D structures of body centred tetrahedral carbon or  $C_4$ . Jun Young Jo and Bog G. Kim [7] predicted the existence of triple bond modified diamond, this is tetrahedral  $C_4$  inserted into the diamond lattice at every carbon atom. This allotrope is semiconducting and may have practical uses if it can be successfully synthesized [8] Carbon is the 4<sup>th</sup> most abundant element in the universe and is the building block of all known life. There are more known carbon containing compounds than any other element.

Carbon nanotubes are structures made of hexagonal units of carbon atoms arranged as a hollow tube, they can be thought of as graphene sheets rolled into a tube shape with the edges of the sheet bound together. They have a diameter ranging in size from approximately 1 nm at their smallest, up to tens of nanometres in multiwall nanotubes. Their length can vary from tens of nanometres to over half a meter. [9] They have different electrical, mechanical and thermal properties depending on how the carbon ring network is aligned with the axis of the tube, known as the angle of chirality. [10] Figure 1 shows the hexagonal carbon ring network that forms the structure of all graphitic materials, specifically CNTs in this case. This figure also illustrates how chiral angle effects the structure of CNTs. They are primarily produced in three ways (1) carbon vapor deposition (CVD), (2) laser ablation, and (3) arc-discharge. CNTs have been produced from a variety of carbon sources including solids [11] liquids [12], and gases [9]. CNTs are formed via the decomposition of a carbon source in the presence of a suitable nanoparticle catalyst. The catalyst material influences the kinetics of the reaction, while the catalyst size greatly influences the state of the product, in that products can range from single walled, multiwalled carbon nanotubes, or carbon fibres. [13]

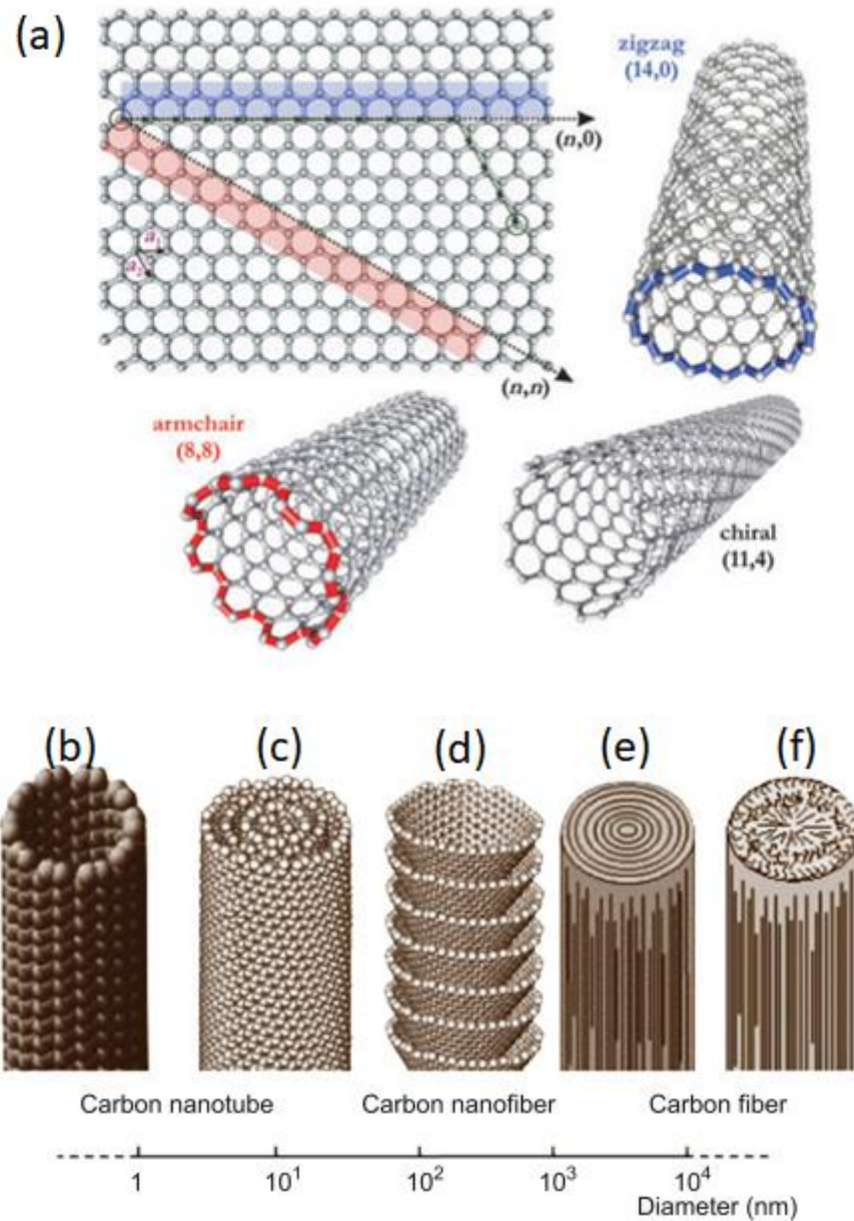


Figure 1: (a) Carbon ring network inherent to all graphitic materials; a graphene sheet may be rolled into a tube with varying degrees of twist based on how the edges are connected known as chirality. The properties of the resulting tubes vary with chirality with armchair configuration tubes being metallic and well suited for conductive applications. [14] Bottom shows size comparison of tubular carbon structures with (b) being a SWCNT, (c) being a MWCNT, (d) being a carbon nanofiber, and (e) and (f) being carbon fibre.[13]

Carbon nanofibers (CNFs), are also made of sheets of graphene. The difference is how the sheets interlock. In CNTs, the graphene sheets can be thought of as rolled in the axial direction with covalent bonds running down the axial direction. CNFs, can be thought of as stacked cones of graphene forming a column or as a continuous spiral ribbon with a hollow core, see Figure 1 (c). [15] CNTs and CNFs form under similar conditions with catalyst particle size determining preference for one form over the other. Catalysts are usually composed of transition metals and metal oxides. Iron and nickel are favoured for catalysts, though CNTs have been successfully grown using non-metal catalyst such as carbon, silicon, silicon carbide, and silicon dioxide. [16] Typical catalyst diameter for growing CNFs is approximately 100 nm. [17] Smaller diameters are more favourable to CNT growth. An iron catalyst size of around 3 nm promotes the growth of a very narrow diameter distribution of SWCNTs. [18] Chhowalla *et al.* described that CNT diameter roughly equalled the diameter of the catalyst particles used for growth. [19]

Current applications of CNTs and CNFs are vast and leverage their excellent mechanical, electrical, and thermal properties. CF embedded in resin is used to make strong, lightweight panels and structural components used in aerospace and automotive design. Current generation aircraft such as the Boeing 787 and Airbus A350 are made of around 50% CF composite materials reducing fuel consumption by up to 25% according to Airbus. [13] The hollow cores in CNTs have been used for hydrogen and gas storage with potential applications in hydrogen fuel cells. [20] CNTs and graphene are widely used in the construction of lightweight lithium-ion battery anodes due to their high irreversible charge storage capacity. [21] CNTs have been used in creating chemical sensors, supercapacitors, and radio antennas. The medical applications of CNTs are promising. CNTs have been used for targeted drug delivery, enhanced imaging, and physical ablation. Due to the dimensions of nanomaterials, they are able to easily penetrate cancer tissues. Because cancer tissues have an ineffective lymphatic system, nanomaterials are not likely to travel to other tissues. This property known as enhanced permeability and retention allows for nanomaterials to be functionalized for specific cancer receptors and concentrated into cancer cells acting as chemotherapy agents without widespread death of healthy tissues. These same properties can also be used to create contrast agents for advanced medical imaging. CNTs can also be used for thermal ablation by radio frequency heating of CNTs in cancer tissues. [22]

C<sub>60</sub> also has great potential in medical and industrial applications. Work done at the Energy Safety Research Institute (ESRI) investigated the use of polyethyleneimine-C<sub>60</sub> for CO<sub>2</sub> capture. [23] Glycoconjugated C<sub>60</sub> (sweet C<sub>60</sub>) has been used with photodynamic therapy to generate reactive oxygen species inside pancreatic cancer cells. Increased glucose demand allowed for the targeted absorption of sweet C<sub>60</sub> by pancreatic cancer cells. [24]

## 1.1 Properties

Carbon nanotubes have potential to innovate many aspects of materials science and research. [25] [26] The electrical properties of CNTs are unique, depending on their chirality, they may be conducting or semi-conducting. [27] CNTs in armchair configuration are known as metallic and are superconducting at low temperatures. [25] They are theorized to have a current density 1000 times greater than copper or silver, 4E9 A/cm<sup>2</sup>. [28] This high current density as well as high tensile strength make CNTs an ideal choice to replace copper and aluminium in transmission lines and electrical circuits.

CNTs are also excellent thermal conductors along their lengthwise axis, due to ballistic transport, which results from very low scattering of electrons through the medium. [29] They also simultaneously have very low thermal conductivity between tubes. From a sheet of aligned CNTs, the thermal conductivity has been measured to be between 25 W/mK and 150 W/mK in plane with longitudinal axis of the tubes while being only 0.1 W/mK out of plane with the tubes. [30] CNTs can also withstand temperatures greater than 4000 K making them very thermally stable, comparable to ultra-high temperature ceramics such as hafnium carbide which has a melting point of 4231 K. [30] [31] Films made from CNTs can be engineered to be either thermally conductive or thermally insulating based on the alignment of the tubes in the film. [30]

They also possess unique mechanical properties. The highest tensile strength material ever measured is a MWCNT, with a tensile strength of 63 GPa. This is over 70 times stronger than stainless steel (SS) while also being 6 times less dense (8.03 g/cm<sup>3</sup> for SS and 1.34 g/cm<sup>3</sup> for CNTs). [32] A defect free CNT is theorized to have a tensile strength of over 100 GPa. Due to defects that form during the CNT growth process, many tubes will exhibit tensile strength far below the theoretical max. Carbon Nanotube Bundles (CNTBs) are groups of CNTs held loosely together by van der Waals interactions. They may be grown in a vertical array or agglomerated post growth.

Because these bundles are made up of individual tubes with different lengths, diameters, and number of defects, CNTBs exhibit much lower tensile strength than individual CNTs ranging from 0.5 to 8.8 GPa. To overcome the inherent weakness of CNTBs, Bai, Y., Zhang, R., Ye, X. *et al.*, produced bundles of ultra-long defect free, CNTs with a tensile strength of 80 GPa. [33]

These properties lead to a vast array of current and potential applications for CNTs. Mechanical applications include composite materials where CNTs are mixed with a polymer to increase material strength. Researchers at Rice University used this technique to produce reinforced biodegradable nanocomposites for bone tissue engineering. [34] CNTs may be formed into a thin film to make an optically transparent conductive surface for use in touchscreens as a replacement for indium tin oxide. [35] The electrical properties of CNTs are leveraged to produce selective bandgap transistors and thin film transistors. CNT thin film transistors are promising for use in transparent drivers for flexible organic light emitting diode displays. [36] CNTs are being evaluated for use as interconnects in integrated circuits due to their exceptional thermal stability as well as their electrical and thermal conductivity. [37]

Carbon fibres (CFs) are typically formed by melt-spinning a polymer filament. Melt spinning is the process of creating very thin filaments via stretching molten polymer using a rotating head. This polymer filament is then thermally annealed at very high temperatures, causing the polymer chain to reorganize into discontinuous fragments of graphene. The diameter of CFs is typically several  $\mu\text{m}$ . CFs are generally spun into threads, which may be further processed into textile or randomly oriented sheets. Strong, lightweight engineering materials are often made of layers of CFs embedded in epoxy. CFs are also added to 3D printing filament to improve mechanical properties.

Vapour grown carbon fibres (VGCF) are CFs that are formed under a hydrocarbon flow at high temperatures using a metal catalyst. A thin carbon filament is first produced by catalytic CVD. This thin filament is then overcoated by many layers of carbon. The diameter range of VGCFs varies from 1 - 100  $\mu\text{m}$ . This process is very similar to the CVD synthesis of CNTs. Unsurprisingly, some VGCFs have been found to have CNTs as their core. [38]

Carbon nanofibers (CNFs) are smaller in diameter than CFs and VGCFs; typically,  $<1 \mu\text{m}$ . They have a more organized structure than VGCFs consisting of stacked planar graphitic layers

resembling a cone (Figure 2-a). CNTs are stacked radially as in Figure 2-b with each layer resembling a cylindrical shell. CNTs are much stronger lengthwise than CNFs due to the covalent bonds that run along the length of the CNT in a zig-zag pattern. The force between the stacked graphitic layers in CNFs is comparable to that between layers of graphene in graphite.

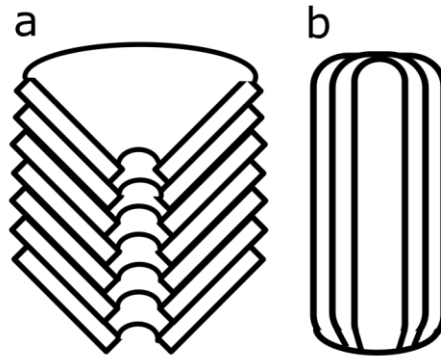


*Figure 2: Cross sectional view of (a) stacked cone CNF and (b) MWCNT. The graphitic planes of (a) stacked in a horizontal arrangement while in (b) they are vertically aligned.*

## 1.2 Growth Methods

Carbon nanotubes are commonly grown through 3 processes (1) arc discharge Figure 3-a [39], (2) laser ablation Figure 3-b [39], and (3) carbon vapour deposition Figure 3-c (CVD) [39].

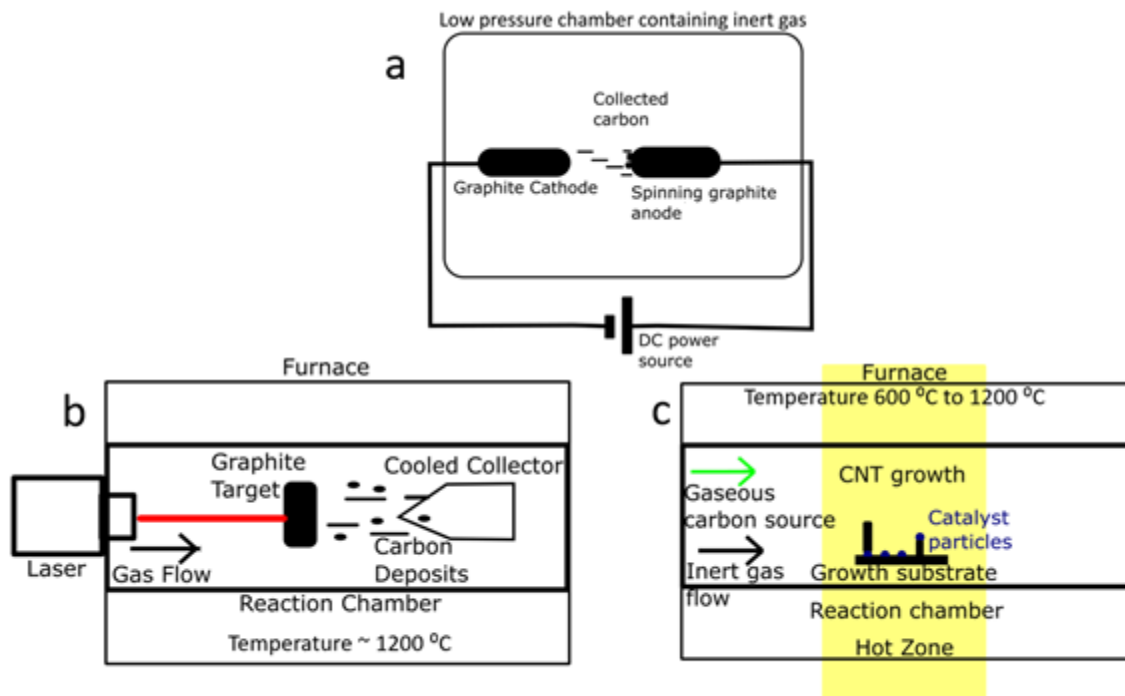


Figure 3: Diagram of CNT growth methods. (a) Arc discharge method. (b) Laser ablation method. (c) Chemical vapor deposition method

Arc discharge is the first method by which CNTs were observed to grow. [40] The system consists of a vacuum chamber, high current power supply, and a pair of graphite electrodes. The electrodes are placed inside the vacuum chamber and separated by a short distance, typically less than 1 mm. The vacuum chamber is filled with an inert gas such as argon and it is pumped down to a low pressure. Then a high current of 50-100 Amps is applied through the electrodes. This current creates a plasma between the electrode tips and a very high temperature ( $>3000\text{ }^{\circ}\text{C}$ ) is reached almost instantly. This causes the decomposition of the graphite and drives the formation of CNTs. This system has the benefit of producing very pure single walled carbon nanotubes (SWCNTs) with few structural defects. However, the drawbacks of this method are



that aligned CNTs cannot be grown, it is difficult to control chirality, and the system is more complex and costly to run compared to the CVD method.

Laser ablation uses a laser to vaporize a graphitic target inside of a furnace set to a temperature of around 1200 °C. The laser heats the graphitic target to high temperature (>3000 °C) .[41] Lasers at 355 nm and 1064 nm have been used to investigate the effect of wavelength on the grown CNTs. [42] The energy of the laser hitting the hot graphitic target causes the formation of carbon radicals that condense as they cool down, to form CNTs on the walls of the furnace as well as on the cooled collector . This process usually forms SWCNTs at low yield with minimal defects and highly defined chirality. This method is also more costly than CVD, requiring expensive lasers and a high electrical power usage.

Chemical vapour deposition (CVD) is the most versatile growth method, allowing for the growth of SWCNT [43], double walled (DWCNT) [44] and multi walled carbon nanotubes (MWCNT) [45], and other carbon species such as carbon fibres and fullerenes. [46] CVD has been used to grow CNTs from solid, liquid, and gaseous carbon sources. CVD relies on the thermal decomposition of a carbon source in the presence of a catalyst, typically from the transition metal series, such as iron or nickel. Because a catalyst is used, this method requires much lower temperatures compared to arc discharge and laser ablation. This makes the system cheaper to run as much less power is required. CVD also allows for much more control of the diameter of grown nanotubes as the size of the catalyst will influence the outer diameters of the materials that are produced. This technique also allows for growth on patterned substrates [47], and to create aligned nanotubes [48], nanotube forests [48], and powders, as well as both thick and thin films [49]. However, one of the drawbacks of this method is that the chirality is hard to control, often resulting in a mix of metallic and semi-conducting nanotubes as well as SWCNTs, MWCNTs and vapour grown fibres under certain growth conditions. The CVD process typically consists of a quartz tube placed inside a tube furnace at a temperature between 500 °C and 1200 °C. An inert gas such as argon is used as a blanket gas in the decomposition of the carbon source. Decomposition of the carbon source takes place on a substrate containing the catalyst. Upon completion of growth, the CNTs are collected from the substrate and the quartz tube after cooling under an argon flow. This is known as a hot-wall CVD reactor. Another variation of the

CVD process is the cold-wall CVD reactor. In this system, the tube furnace that heats the quartz tube and substrate externally is replaced with a heater that heats the substrate directly. This method allows for even lower power consumption and greater control over the temperature of the substrate due to the very localized heating. These systems also have the advantage of a lower process time as the substrate can heat and cool more rapidly. As such, the cold walled CVD system was chosen in this work for use in the growth of carbon nanomaterials to test multiple parameters with a rapid throughput.

Regardless of the CVD reactor geometry, catalytic growth of CNTs occurs when a carbon source is pyrolyzed and absorbed onto catalyst particles. When the carbon source vapour encounters the heated catalyst nanoparticle, the carbon source is decomposed into the base elements, active  $C_xH_y$  radicals and atomic carbon. [50] In the case of camphor, the decomposition process yield carbon, hydrogen, and oxygen radical. The hydrogen combines to form  $H_2$ , which is carried away when the reactor is flushed post growth. The carbon is dissolved onto the surface of the catalyst particle forming a solid solution. When the catalyst surface is saturated with carbon, carbon starts to precipitate at the surface and begins to form planar hexagonal carbon on the particles' surfaces. [50] Oxygen may combine with hydrogen to form water which may help keep the catalyst surface free of amorphous carbon and increase the catalyst lifetime. Water concentration has a direct impact on catalyst activity. [9] Low water concentrations are unable to remove all the amorphous carbon and decrease catalyst lifetime. Too much water will also remove unreacted carbon decreasing the supply and limiting the reaction. [9] Oxygen may also combine with excess carbon to form  $CO_2$  which also helps keep the catalyst active. If the catalyst is bonded strongly to the substrate, the carbon will precipitate on top of the particle and CNTs will form growing away from the substrate, known as root growth. If the catalyst is weakly attracted to the substrate, the carbon will precipitate over the whole catalyst particle and growth will initiate on the bottom, carrying the catalyst away from the substrate as the CNT grows, known as tip growth. It is also possible for the particle to initiate growth from both the top and bottom leaving a catalyst particle somewhere along the length of the tube but not on either end.

### 1.3 Analytical techniques

Carbon nanotubes (CNTs) are primarily identified by their Raman spectrum. [10] They are also visually observed by scanning electron microscopy (SEM) [51] and transmission electron microscopy (TEM) [51]. Energy-dispersive X-ray spectroscopy (EDS) may also be used to perform elemental analysis of samples and catalysts. [52] Large bundles may even be observed by the naked eye. This work relies solely on SEM, EDS, and Raman spectrography for analytical techniques; for clarity an overview of TEM is also presented below.

Raman spectroscopy is an analytical technique that observes the interaction of light with matter known as Raman scattering. This technique allows for the observation of a samples molecular structure and vibrational state. Raman scattering is an inelastic scattering process, meaning that the incident photon's kinetic energy is not conserved. An incident photon with energy  $E_{\text{photon}} = h\nu$ , where  $h$  is Plank's constant and  $\nu$  is frequency in Hz, excites a molecule from an initial vibrational state to a higher virtual state, a very short-lived and unobservable quantum state. The molecule then relaxes to a vibrational state lower than the virtual state but higher than the initial state by emitting a photon with energy  $h\nu - \Delta E$ , where  $\Delta E$  is the energy difference between the initial and relaxed state. This is known as Stoke's scattering. Inelastic scattering can also result in the emission of a photon with energy  $h\nu + \Delta E$ , known as anti-Stoke's scattering. For this to occur, the molecule starts in an already excited state, the incident photon further excites the molecule to a virtual state. The molecule relaxes to an energy state lower than the initial state by emitting a photon with higher energy. Rayleigh scattering is the elastic scattering of a photon, this happens when a molecule is excited to a virtual state and relaxes back to its original state. The incident photon and the emitted photon will have the same kinetic energy. Inelastic scattering events are very rare occurring in approximately 1 in 10 million scattering events. Raman shift is reported in wavenumbers and given by the formula bellow, where  $\Delta\tilde{\nu}$  is the Raman shift with units of inverse length (1/cm),  $\lambda_0$  is the excitation wavelength (nm), and  $\lambda_1$  is the Raman spectrum wavelength (nm). Equation 1 shows the relationship between wavelength and wavenumber.

$$\Delta\tilde{\nu} = \left( \frac{1}{\lambda_0} - \frac{1}{\lambda_1} \right)$$

*Equation 1*

Raman spectroscopy systems use a monochromatic light source, usually in the near-infrared or visible spectrum, to excite the sample. The spectra are obtained by measuring the intensity of the emitted light as a function of energy shift. This is represented as a wavenumber shift from the incident light in  $\text{cm}^{-1}$ . As the Raman shift is independent of the incident light's wavelength, different wavelength sources can be used to obtain the same Raman spectra, allowing for the selection of a wavelength that is not well absorbed by the sample and avoids issues such as fluorescence. [10] Raman spectroscopy measures the intensity of emitted photons at each shifted wavelength. As the intensity of the Raman shifted signal is very low compared to the intensity of the light source, a notch filter is used to reject light.

In the Raman spectra of carbon nanomaterials there are three distinct peaks that represent different bond types between carbon. In 2D graphene, there is a peak around  $1582 \text{ cm}^{-1}$  known as the G band/peak, also known as the graphite band. This peak results from the interaction of the laser light with  $\text{sp}^2$  bonded carbon atoms. [10] All allotropes of carbon with a crystalline hexagonal lattice express  $\text{sp}^2$  orbital hybridization this means that CNTs, CNFs, graphene, graphite, and fullerenes display the G band. The D band, also called the disorder band, is around  $1350 \text{ cm}^{-1}$  and represents defects in the graphene lattice as well as graphene edges. Isolated SWCNTs will show a very weak D peak or none at all, due to the continuous  $\text{sp}^2$  bonded carbon that make up the walls and ends of the tube. The ratio of G to D peak intensity is used as a marker of the quality of tubes produced, [53] where a larger G:D ration implies higher quality CNT samples. A very large D peak usually indicates the presence of amorphous carbon or defects in the CNT material. The G' band, also known as the 2D band, is located at  $2700 \text{ cm}^{-1}$  and is formed independent of defects. Amorphous carbon and graphite may have a slight 2D peak or none at all. Figure 4 shows the Raman spectra obtained from a liquid injection CVD reactor (LIR), where m-cresol and ferrocene are injected at a constant rate into the reactor hot zone. This allows for the carbon source and catalyst to be renewed and for the reaction to run indefinitely as long as the carbon deposition is collected at a constant rate. This constant growth method allows for a higher yield as the reaction chamber does not have to be heat cycled between every batch. The

bottom plot in Figure 4 shows the Raman spectra obtained from commercially available carbon fibres (FibreGlast L210530).

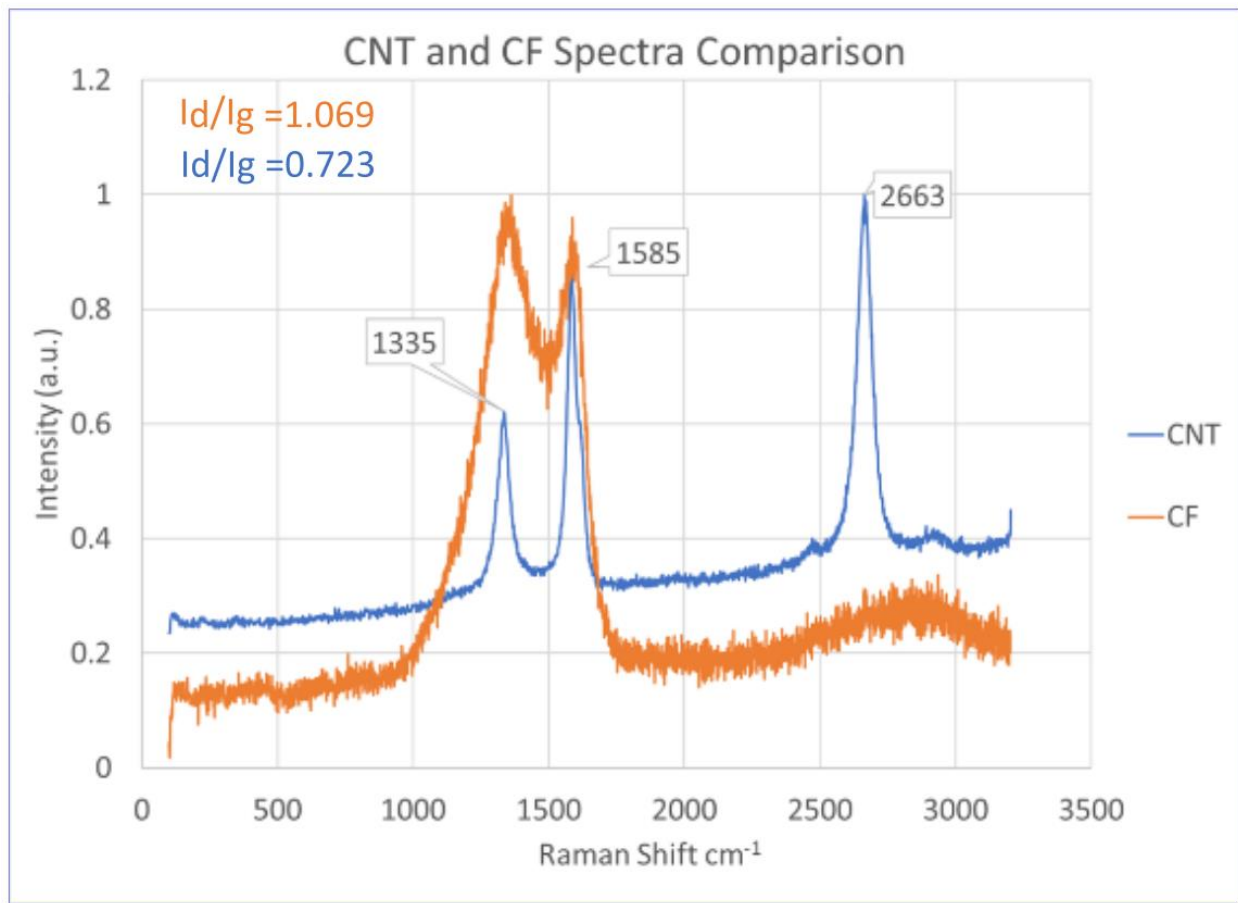


Figure 4: Raman spectra comparison of CNTs (in blue) obtained via liquid injection reactor synthesis and commercially obtained CFs (FibreGlast L210530) (in orange). The  $I_d/I_g$  ratio is displayed on the graph in corresponding colours. Notice lack of peak around 2700  $\text{cm}^{-1}$  on CF spectra. This is the primary difference between the two spectra. All Raman spectra were obtained using 633 nm laser at 10% power with a 30 second acquisition time.

Raman spectroscopy provides a unique set of peaks and valleys allowing for identification of a compound based on bond type and symmetry. Because CNTs and graphitic carbon allotropes are composed of the same building block,  $\text{sp}^2$  hybridized carbon in a hexagonal crystalline lattice, the differences between carbon allotropes may not be readily apparent. Impurities and defects in a sample may obscure its true nature. Therefore, another complimentary method is useful for final determination of the sample. Typically, scanning electron microscopy (SEM) and transmission electron microscopy (TEM) are used. TEM is a direct imaging technique in that

transmitted electrons form an image or diffraction pattern that can be recorded directly to film or a charge coupled device (CCD) camera. SEM relies on a pencil shaped electron beam that scans the surface in a pattern. An electron detector measures the electrons that are scattered by the surface of the sample where the beam terminates. After the surface is scanned, an image is created by combining the measured scattered electrons using software. The image is then displayed on a viewing screen. TEM is capable of greater resolution than SEM, typically 0.5 Angstrom. SEM has a resolution of about 4 Angstrom

Transmission electron microscopes are similar to optical transmission microscopes in that they use a lens to focus a beam from a large diameter column to a cone terminating on the sample as a point, the difference is that TEM uses electrons and optical microscopes use photons. The larger the aperture lens and the shorter the wavelength of the light source, the smaller the point can be made on the sample. The area illuminated on the sample forms an image on the other side of the lens that is enlarged by a magnification factor  $M$  given in the equation below, where  $f$  is the focal length,  $u$  is the distance between the object and the lens, and  $v$  is the distance between the lens and the enlarged image. Equation 2 represents the mathematical relationship between these variables while Figure 5 represents them visually.

$$M = \frac{f}{u - f} = \frac{v - f}{f}$$

Equation 2

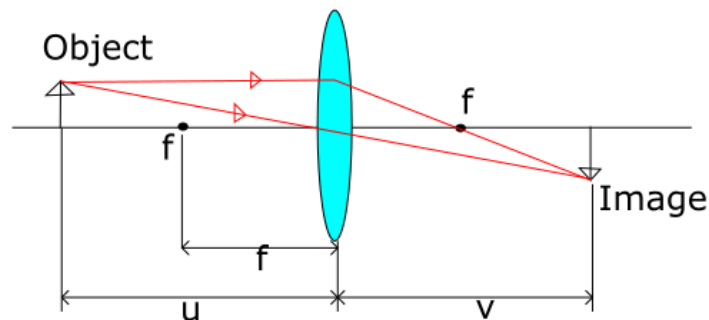


Figure 5: Magnification equation and diagram relating focal length with objective diameter.

TEM uses a very thin wafer of sample as it must be able to transmit electrons through the sample. Transmitted electrons are used to reveal the internal structure of a sample such as the number of layers in a MWCNT. SEM and TEM require the samples to be conductive in order to

be imaged effectively. If a sample is not conductive enough, the surface of the sample will begin to store excess electric charge due to the build-up of electrons. The surface charge will deflect the electron beam obscuring the point of interest. Both CNTs and CNFs have the appearance of hair-like filaments under electron microscopy. Graphene appears as a 2D planar structure and is easily distinguishable. Graphite is composed of stacks of graphene held loosely together by interlayer Van der Waals forces. Observing CNTs in SEM or TEM requires special attention to detail during sample preparation. Samples grown using CVD can have a very high amount of amorphous carbon making observation difficult. It is often necessary to clean up samples by washing with a solvent such as acetone. Typically, after a sample is washed with acetone and dried, a small amount (<5 mg) of the sample is mixed in ethanol (~10 mL) and dispersed by sonication for up to 30 mins. The sonicated sample is then pipetted onto an aluminium SEM stub or copper TEM grid and allowed to dry for around 24 hours in a desiccator in advance of placing in the SEM vacuum chamber. After drying, the sample is ready for observation. Figure 6 shows an SEM image of CNTs grown using LIR. This sample shows fibres of different diameters grown together in a random orientation. Several of the fibres appear to have lumpy nodules likely resulting from being coated in amorphous carbon and catalyst particles.

Scanning electron microscopy allows for the observation of the surface topography of a material as well as its composition at a much higher resolution, the smallest identifiable distance between two features, than optical microscopy. The higher resolving power is due to the fact that the wavelength of an electron can be 100,000 times shorter than that of visible light allowing for the viewing of smaller objects. Whereas a visible light microscope uses a convex lens, often made of glass, to guide photons to converge on the focal point, an electron microscope uses electromagnetic fields to form a lens capable of guiding electrons. Electrons are absorbed by air; this means that an electron microscopy sample must be viewed under vacuum to maximize resolution. SEM uses the interaction of high energy electrons with the sample's surface to generate ionization products known as secondary electrons. This is the main way of viewing a sample in a SEM. Another viewing mode for SEM uses backscattered electrons to image a sample. Backscattered electrons (BSEs) are generated when an electron in the primary beam travels very close to an atomic nucleus in the sample. The interaction of the positively charged nucleus and

the negatively charge electron generates a force that deflects the primary beam electrons by an amount proportional to the atomic number of the surface atoms, higher atomic number causes more electrons to be deflected towards the BSE detector. The measured number of BSEs reveals information about the composition of the sample's surface.

Another analytical technique used to help characterize CNT samples is EDS. EDS uses a focused beam of X-rays to excite a sample causing the emission of characteristic X-rays from atoms in the sample. The incident beam excites an electron in the inner shell of an atom ejecting it and creating an electron vacancy. A higher energy electron from an outer shell fills this vacancy while releasing energy in the form of an X-ray. The amount of energy released is characteristic of each element allowing for elemental composition of a sample to be measured.

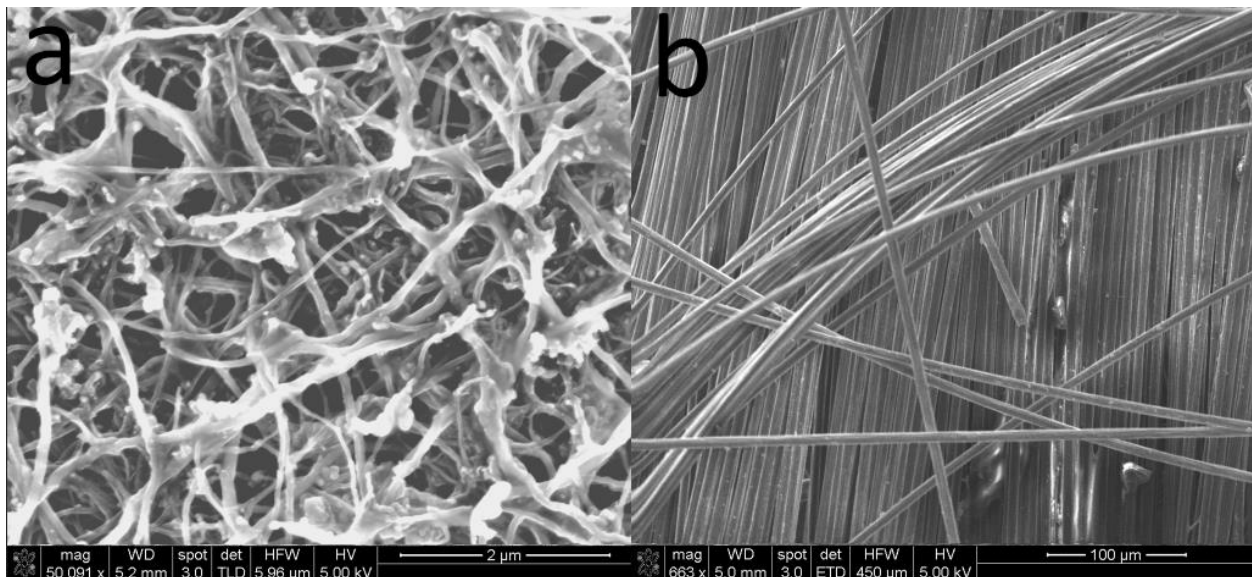


Figure 6: (a) SEM of as-grown LIR CNTs, (b) SEM of commercial CFs from an aligned sheet

## Chapter 2: Reactor Construction

### 2.1 System Diagram and Schematics

Chemical vapour deposition (CVD) reactors are one of the most studied production methods for CNT growth. In hot wall CVD, a quartz tube is placed inside a furnace to create a zone of nearly constant temperature, known as the hot zone. These systems are widely used in the semiconductor and optical coating industries. In a hot wall CVD reactor, the carbon source, usually carried by an inert gas, is passed over a substrate in the hot zone of the reactor. The heat decomposes the carbon source and reacts the carbon radicals with a catalyst to form nanotubes.



This system has a higher energy footprint and initial setup cost when compared to a cold wall CVD reactor. A cold wall CVD reactor does not require a furnace to heat the substrate eliminating a lot of thermal mass that must be heated to reaction temperature and thus reducing the heating time and energy use of the system. Cold wall CVD reactors use a much smaller heater that is attached directly to the substrate. This allows for the use of materials that are not as well suited to hot wall reactors such as solid carbon sources. Eliminating explosive gases from the system also improves safety and reduces costs associated with gas monitoring and plumbing. A cold wall system also allows for the use of both solid and gaseous carbon feedstock, thus allowing a large variety of input materials. The walls of the quartz tube were never observed to glow red indicating that the temperature was less than 480 °C, the temperature at which incandescence becomes noticeable. This is especially important given the fact that several non-recycled carbon materials are solids, such as plastics and other biomaterials. The use of a cold wall CVD using camphor as a test case allows for baseline testing and development for future reactions with more exotic carbon sources. With this in mind, a cold wall CVD reactor was chosen for this study.

The system consists of a 1 meter long 50 mm OD quartz tube with SS flanges (MTI Corporation) on each end. The tube rests on 3D printed supports to keep it elevated from the work surface. The input side flange is a 1/4-inch threaded tapered nozzle with a screw valve. The input side flange also has a 1/4 inch hole drilled in it for wire access. The output side flange is connected to a water bubbler. The heater assembly rests in the middle of the quartz tube. Wires pass through the input side and connect the heater (16-gauge wire) and thermocouple (30-gauge wire). The heater is connected to a relay that is across the output of the variable AC transformer and controlled by PID to maintain a set temperature. Figure 7 shows a broad electrical overview of the system. The whole system is placed into a fume hood.

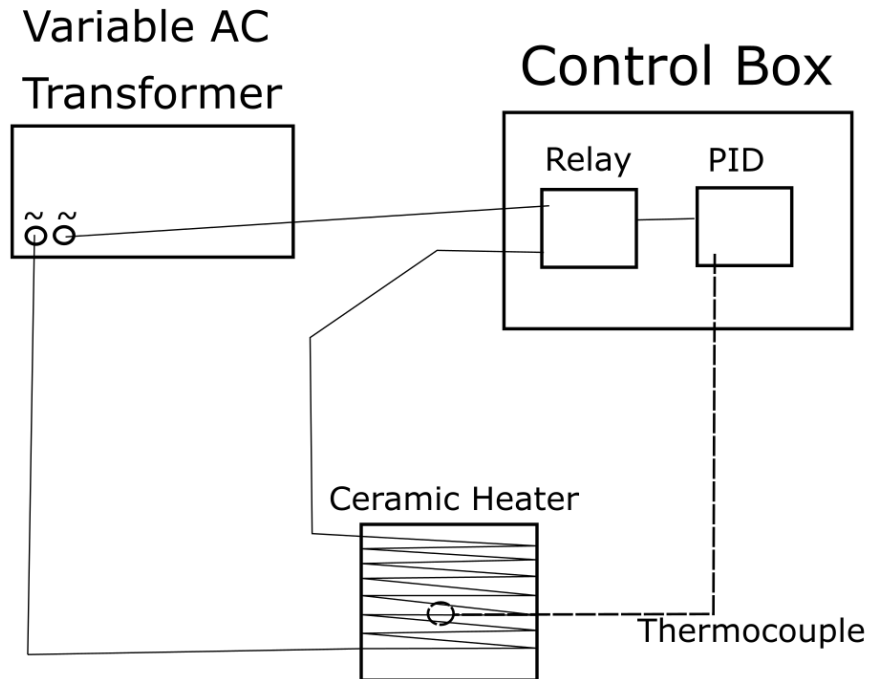


Figure 7: Electrical overview of the designed cold wall CVD system

## 2.2 Materials Selection

There is an ever growing need to find alternative remediation routes for waste carbon materials. Climate change due to atmospheric carbon emissions is a major threat to life as we know it. [54] Plastics and rubbers take up space in landfills and often end up in the ocean instead of being recycled. As plastics and rubbers are forms of solid carbon sources, it would be valuable to devise a cheap and easy method of converting them to useful materials. As such, it was determined that starting with a solid carbon source could provide valuable insight into CNT and CNF growth from polymer waste. Previous work has shown that camphor has been used successively for CNT growth [11], as such it was deemed an appropriate initial carbon source for the cold-wall CVD system. There is less work using solid carbon sources but Kumar *et al.*, have demonstrated controlled growth using camphor. Camphor is a waxy terpenoid found in the wood of the camphor laurel, an evergreen tree from Southeast Asia. Camphor has also been used for

centuries for its medicinal, culinary, and fuel applications. [55] Camphor also has the benefit of being a renewable resource allowing for the production of CNTs without petroleum.

The camphor molecule has 10 carbon atoms consisting of 3 methyl groups attached to a 3-dimensional structure consisting of a pentagonal and hexagonal carbon ring (Figure 8). During decomposition, atomic carbon and  $C_xH_y$  radicals form. [50] If these radicals find a correctly sized catalyst particle at the correct temperature, they will form into carbon nanotubes. Camphor also has an oxygen atom; I speculate that the oxygen may combine with hydrogen and form water which may be useful in removing or preventing amorphous carbon build-up from fouling the catalyst particle that would otherwise form metallic carbides [9]

Zeolite is a mineral consisting of aluminosilicates arranged into porous cubic crystals. Zeolite was chosen as a substrate because it increases the surface area for catalytic sites to form on versus a planar structure. The zeolite is also stable at the reaction temperature.

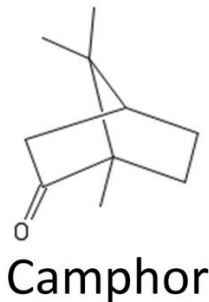


*Figure 8: Skeletal structure of camphor molecule. Camphor has a hexagonal carbon ring with a carbon atom splitting the middle, forming two pentagonal rings. Functional groups consist of three methyl and one ketone group. The aromatic carbon rings help in the formation of carbon ring free radicals that are the direct building blocks of CNTs. The oxygen atom may help prevent catalytic fouling by combining with amorphous carbon to form gaseous carbon oxides.*

Temperature is an essential parameter of CNT growth. Therefore, having proper heat production and control is important. Typical reaction temperatures occur between 550 and 1000 °C and may be sustained up to several hours. After testing several commercially available ceramic heaters, it was decided to design and fabricate a custom heater. The tested commercial heaters could not handle the high electrical power demands (1000 Watts peak) and failed to reach and maintain a suitable temperature.

The custom-made heater consists of a quartz plate wound with braided NiCr wire embedded in a polymer matrix ceramic resin and sintered in a kiln to 1270 °C. This heater is powered by a variable output AC transformer. Figure 9 shows a 3D CAD rendering of the quartz reaction chamber. Heating control is achieved through the use of a thermocouple and PID controller that cycles the output of the transformer. This heater was tested and able to withstand more than 20 temperature cycles up to a temperature of 750 °C. This heater was able to reach 600 °C in less than 3 minutes at max power (Figure 10).

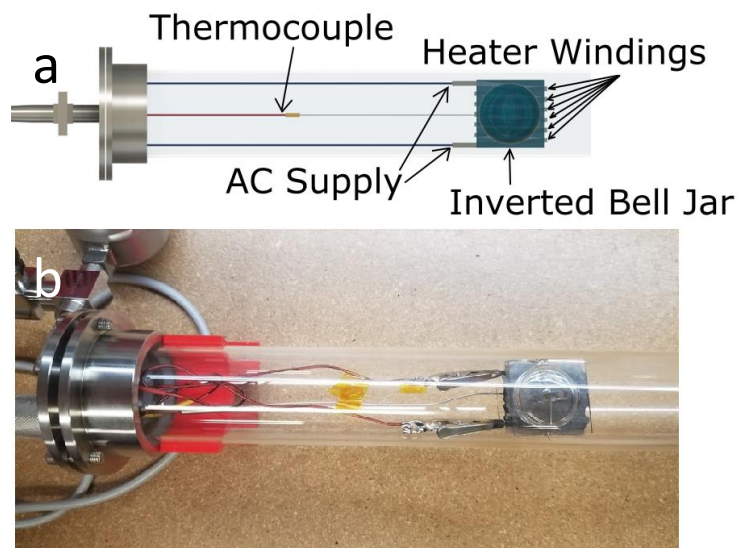


Figure 9 (a) 3D render of ceramic heater design (b) photographic overview of same

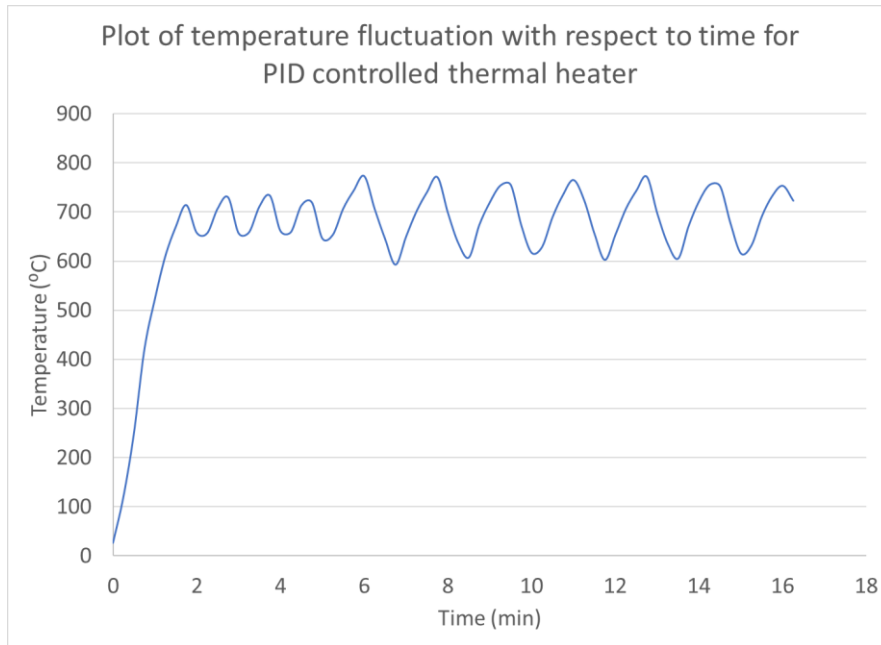


Figure 10: Ceramic heater temperature plot for sample 6. System displays oscillation possibly due to incorrect PID tuning. This temperature variation will increase the growth rate at higher temperatures [56]

Having already designed and constructed the heater with a 2-inch diameter quartz tube in mind, a 1.5-inch square x 1/16-inch quartz plate was selected as a substrate holder. This is placed directly on top of the ceramic heater. A thermocouple is sandwiched between the bottom of the ceramic heater and another quartz plate. The placement of the thermocouple is important in order to be measuring at approximately the centre of the heater. Placing the thermocouple too close to the edge will read a lower temperature than one placed in the centre. The heater must also be examined for large cracks and exposed windings as this can cause a short circuit between the thermocouple and the heater. The carbon source and catalyst are placed on top of the quartz substrate holder. The ferrocene catalyst is mixed with zeolite at 5 wt%. Zeolite is used as a substrate material that helps adjust the concentration of ferrocene. An inverted bell jar is placed over the carbon source and the whole heater assembly is twisted together with tie wire. Figures 9 and 11 show a schematic of the heater assembly.

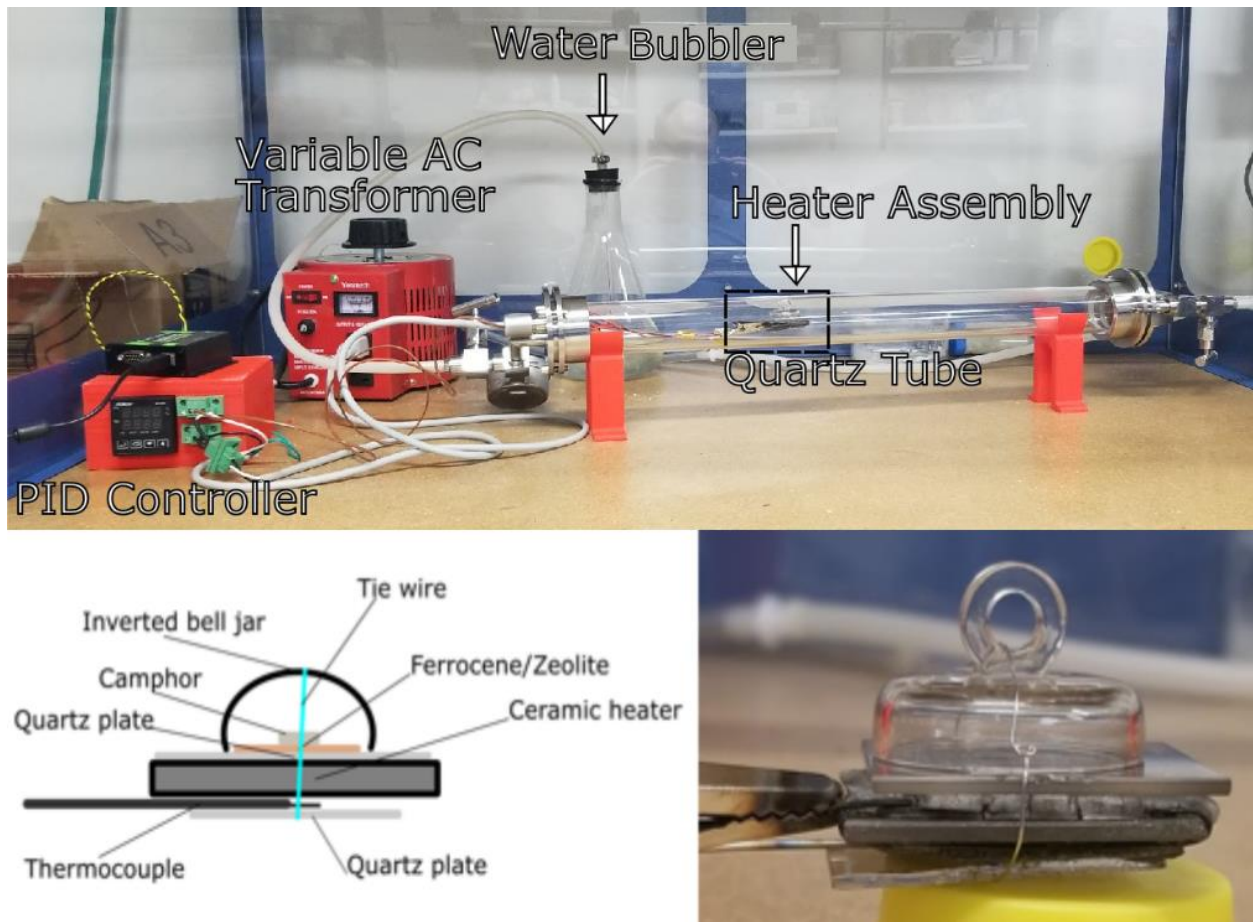


Figure 11: (a) Cold wall CVD reactor constructed in Houston, Texas (b) side view of heater assembly with labelled components (c) magnified photo of boxed region in image (a) showing side view of heater assembly

The ferrocene concentration as well as the reaction time and temperature determine the diameter of the iron catalyst particles produced and ultimately this determines if CNTs or CNFs are grown as well as the fibre diameter. [38] Catalysts are typically transition metals with iron being used heavily. Iron has the advantage of high catalytic activity while also being less toxic than other commonly used metals such as nickel and cobalt. The metals must be formed into nanoparticles and distributed over the substrate. If the concentration of catalyst is too high, Ostwald ripening will occur causing the smaller nanoparticles to join together into larger particles which can change the synthesised product from CNTs to CNFs. The nanoparticles may be patterned onto the substrate using lithography techniques or be created in-situ by

decomposition of metal-containing molecules. Ferrocene (Figure 12) has been widely used as a precursor for iron nanoparticle formation. Ferrocene is a metallocene molecule with an iron atom sandwiched between two cyclopentadienyl rings. A metallocene is a molecule with two cyclopentadienyl anions bonded to a metal in the centre. Kumar *et al.* [11] determined the ideal ferrocene concentrations for growing CNTs from camphor on zeolite substrate, although they used a hot-wall furnace design. They determined that the ideal catalyst concentration for growing SWCNT was 2.4 wt% in zeolite and the ideal concentration for MWCNTs was 9 wt%. They noted a mix of SWCNT and MWCNT at ranges between these numbers. Five wt% ferrocene in zeolite was selected as a constant to understand the effect of temperature on the growth characteristics in a cold-wall reactor. Five wt% was selected as a compromise between favouring the growth of SWCNT and MWCNT as well as to avoid having too low of a concentration as Kumar *et al.* [11] determined that no CNT growth occurred at catalyst concentration less than 2.4 wt%.

Upon decomposition, the cyclopentadienyl rings break away and decompose further into carbon and hydrogen radicals leaving behind elemental iron. With in-situ nanoparticle production, the ferrocene is mixed with an inert carrier substrate such as zeolite. The ratio of ferrocene to zeolite as well as temperature determines the size and concentration of the nanoparticles formed.

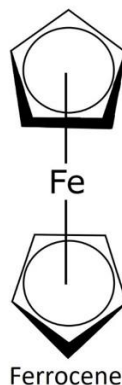


Figure 12: Ferrocene molecule, consisting of central iron atom sandwiched between 2 cyclopentadienyl rings. High temperature decomposition yields iron nanoparticles that act as a catalyst for the CNT and CNF growth process. The size of iron nanoparticles is determined by ferrocene concentration, temperature of reaction, and time held at temperature. Diameter of catalyst particles determines whether CNT or CNF are grown as well as their resulting diameter.

## 2.3 Growth Parameters

Many parameters effect the growth of graphitic materials such as CNTs and CNFs. The most important factor determining diameter of grown samples is catalyst diameter. Cheung *et al.* [18] describe diameter-controlled growth of CNTs. They prepared iron nanocluster of a very narrow diameter distribution by thermally decomposing iron pentacarbonyl in the presence of oleic acid, lauric acid, or octanoic acid, which acts as capping ligands limiting the size of nanoparticles as they form. These acids formed average diameter particles of 3.2 nm, 9 nm, and 12.6 nm, respectively. They demonstrated that larger catalyst particles lead to larger diameter nanotubes with the 3.2 nm particles producing CNTs of 2.6 nm diameter, and the 9 nm and 12.6 nm, nanoparticles producing CNTs of 7.3 nm and 11.7 nm average diameter, respectively. These CNTs were produced using CVD with ethylene or methane as the carbon source. Temperature has a large impact on diameter of grown CNTs. Higher temperatures favour larger diameter CNTs. [57] This is due to increased Ostwald ripening with increasing temperature, causing smaller catalyst particles to agglomerate forming larger particles. Temperatures below 700 °C result in very little CNT growth due to limited catalytic activity. Temperatures greater than 1000 °C result in deposition of high amounts of amorphous carbon as well as CNTs. Growth time is also an important factor. Process times lower than 15 min were found to result in a high number of defects in the grown CNTs. Longer process times favour the growth of higher proportion of smaller diameter tubes compared to shorter process times. Navas *et al.* propose this is due to dynamic competition between Ostwald ripening and nanotube growth. [58] Larger catalyst particles are terminated first by catalytic poisoning while smaller nanotube growth is terminated by Ostwald ripening.



## Chapter 3: Growth Protocol and Results

### 3.1 Growth Protocol

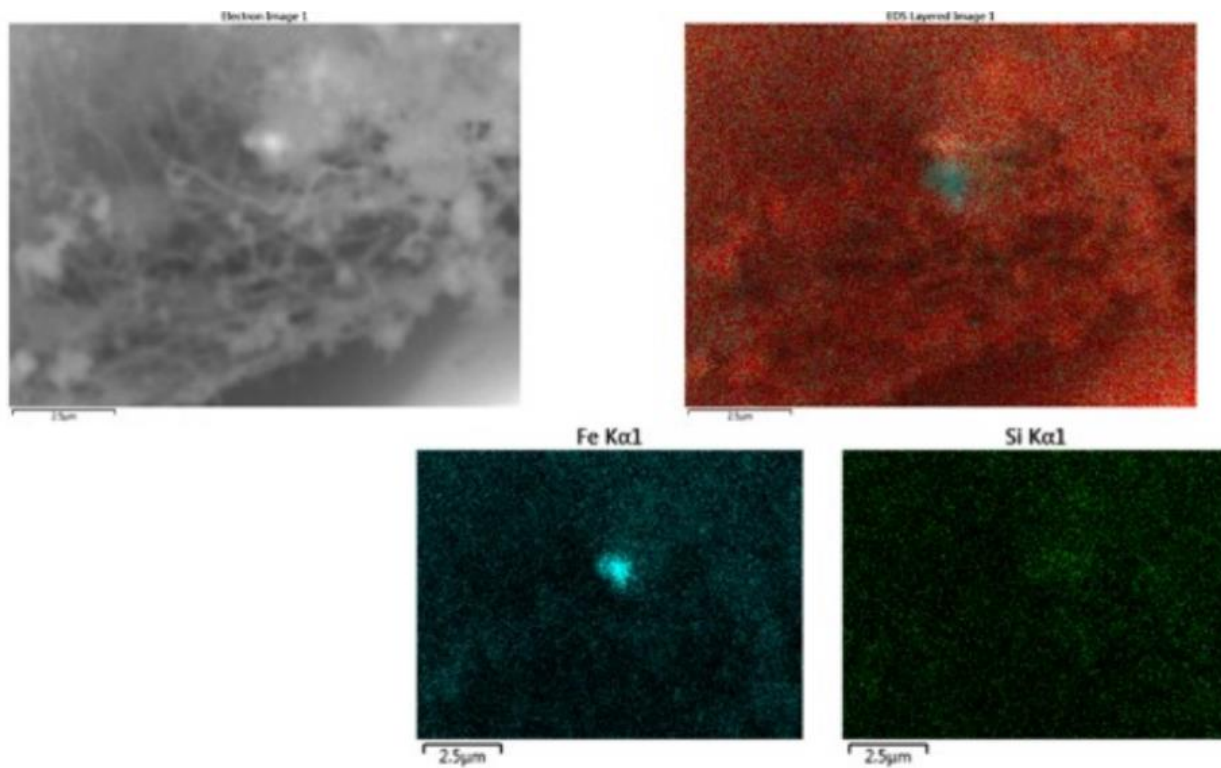


Figure 13: EDS elemental analysis (performed on Hitachi desktop SEM) showing presence of iron (cyan), carbon (red), and silicon (green) confirming that ferrocene was decomposed into catalyst particles. Silicon is used to visualize zeolite as it is an aluminosilicate material.

Camphor (97% Sigma-Aldrich 148075) is used as the carbon source. Bulk zeolite (Sigma-Aldrich 96096) is used as a catalyst support. Ferrocene (Sigma-Aldrich 98% F408) is used as the catalyst. Energy-dispersive X-ray spectroscopy (EDS) Figure 13, is performed to determine the elemental composition of a sample (using equipment at the ESRI in Swansea, Wales.) The catalyst is prepared by weighing out ferrocene in concentrations of 1 to 50 wt.% in zeolite. The ferrocene is dissolved into 20 – 50 mL toluene and sonicated with the zeolite powder for 10 min. The mixture is then dried on a quartz petri dish at 60 °C for 2 hours then ground and mixed by hand. Each run, 50 mg of camphor and 50 mg of zeolite mixture are placed on the quartz plate substrate. A quartz bell jar is placed over the top of the powder. The whole assembly is then wired shut with NiCr wire and placed into the centre of the 50 mm O.D. quartz reaction tube. The quartz tube is flushed with Ar for 10 min at 300 sccm to create an inert atmosphere within the

tube. The outlet of the quartz tube is piped through a water bubbler to reduce particulates. The gas flow is then reduced to zero. The variable AC transformer is set to 40 V<sub>AC</sub>. The PID controller is set to the desired temperature and set to run. The temperature is observed to rise rapidly with visible vapour forming in the tube within 30 seconds. The set temperature is achieved within 5 minutes and this temperature is held for 15 min. After the hold time, the power is removed from the heater circuit. The Ar flow is returned to 300 sccm and the reactor is allowed to cool to room temperature under Ar flow. The Ar flow is reduced to zero. The sample is removed from the substrate and analysed using Raman spectroscopy and SEM.

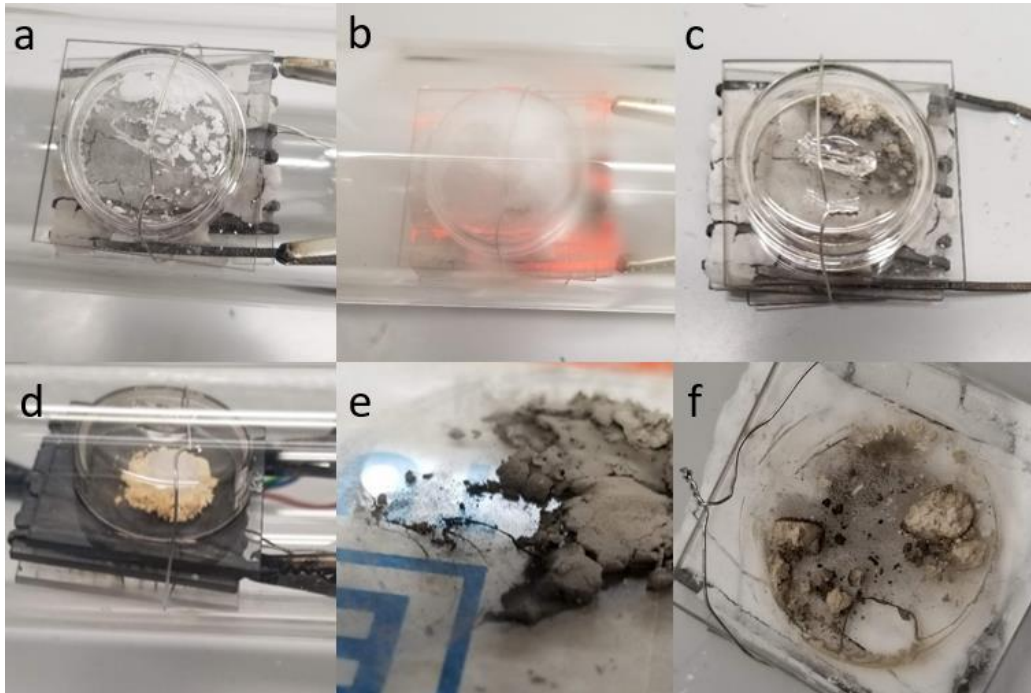
Figure 13 shows EDS analysis of sample 4 grown at 700 °C. This technique is used to observe the elemental composition of a sample. This technique uses an X-ray source to interact with the sample and generate a spectrum. The X-ray interacts with an electron in an inner shell of an atom and ejects it. This causes a hole vacancy to form at that location and an electron from an outer, higher energy shell moves into the vacancy. When the electron moves from an outer shell to inner one, excess energy is released in the form of an X-ray. The energy of the X-ray is equal to the difference in energy between the two shells and is unique to each element allowing for identification.

Figure 14 shows the progression of the sample during a typical growth. Figures 14-a and 14-d show the sample pre-growth, Figure 14-a is a control sample without ferrocene while Figure 14-d is with ferrocene. Ferrocene has a red-brown crystalline appearance. It quickly sublimates at room temperature so care must be used that samples are not left out in the open for too long. When the ferrocene is mixed with the white zeolite, it makes a light orange powder. Camphor has a waxy crystalline appearance and is off-white. The zeolite/ferrocene mixture is placed onto the 38 mm square quartz plate and slightly flattened with a spatula to increase the surface area and contact between reagents. The camphor is then placed on top of and beside the zeolite/ferrocene mixture. The 3 mL inverted bell jar is then placed on top of the powders and wired shut with 0.32 mm diameter NiCr wire. The ceramic heater is also visible in most of the images. This heater was custom fabricated using a 38 mm square 1.6 mm thick fused quartz plate as the core. Braided NiCr wire with a rectangular cross-section was selected as the heating element. Braided NiCr was selected as opposed to a solid strip as the braided wire was easier to

shape by hand and has a very favourable electronic characteristics as it was designed specifically for low voltage, high current heating applications. This wire was wound by hand around the quartz core a total of eight times resulting in a resistance of  $1.6 \Omega$  measured using a digital multimeter. The wire was allowed to protrude 15 mm from the quartz plate to facilitate connecting the power supply via alligator clips. The core was then coated in ceramic resin (Form Labs, Inc.). This resin is a liquid polymer and ceramic particle suspension. The exact composition is proprietary. This resin is cured using 405 nm UV light forming a solid polymer-ceramic matrix. This process was repeated until the NiCr wire was sufficiently coated. Sanding was used after curing to form a flat face that would allow effective and uniform heat transfer to the growth plate. After the heater was cured and sanded, the ceramic must be sintered in a kiln or box furnace. The polymer resin must first be burned off by holding the temperature at  $300 \text{ }^\circ\text{C}$  for 10 hours. After the polymer is burned off, the ceramic particles are loosely held together and must reach a temperature of  $1270 \text{ }^\circ\text{C}$  to be bonded together. The temperature must not be increased too fast or the ceramic will fracture. The temperature must then be slowly lowered before the heater is ready for use.

Figure 14-b shows the camphor vapor cloud that forms while the growth temperature is being reached. The vapor can clearly be seen escaping the inverted bell jar and coating the quartz tube. Once the sample reaches the set temperature, the haze of the camphor disappears from the quartz tube and the inverted bell jar. After 15 minutes at the set temperature, power to the heater is disconnected and the sample is allowed to cool naturally under a light argon flow; 200 sccm. Figure 14-c shows the heater assembly post growth after being disconnected and removed from the quartz reactor tube. The NiCr wire is cut and the sample is collected using a spatula. Figures 14-e and 14-f show the as-grown sample before being collected. Notice that there are differences in colour in the sample between black and light grey. Figure 14-e shows a sample where the zeolite was flattened while image Figure 14-f shows a sample where the zeolite was more clumped together. The colour of the sample seems to correspond to the thickness of the zeolite substrate. The closer the zeolite was to the quartz growth plate, the darker it was. This is due to a temperature gradient that must exist as the further away from the growth plate it is the cooler the temperature will be. I speculate that the temperature gradient results in different

concentrations and sizes of catalyst particles resulting in more CNT and amorphous carbon growth in the higher temperature region closest to the quartz growth plate. This explains the darker colour of the sample closer to the plate.



*Figure 14: (a) growth plate before heat application, (b) growth plate during heat application, (c) bell jar wired to growth plate post run, (d) growth plate with heater stage discoloration after many runs. (e) close up of growth plate sans heater post run. (f) close up of heater stage after first run. This visualizes a time lapse of the process.*

### 3.2 Results and Discussion

To determine a baseline from which the temperature should be set, several runs were conducted at 550, 600, 650, and 700 °C using 5 wt% ferrocene in zeolite. Using Raman spectroscopy, each sample was characterized at between 5 to 10 random locations and an average normalized spectrum was obtained. A typical CNT Raman spectrum (Figure 4) will have 3 peaks centred at  $\sim 1582\text{ cm}^{-1}$  (G band),  $1350\text{ cm}^{-1}$ , (D band), and  $2700\text{ cm}^{-1}$ , ( $G'$  band). As previously stated, the G band is known as the graphitic band and results from the interaction of laser light with the  $sp^2$  bonded carbon. This peak is present in all  $sp^2$  bonded carbon allotropes and therefore cannot differentiate between CNTs, CNFs, graphite, and graphene. The D band results from interactions of laser photons with disorders in the graphene lattice. Disorder may

consist of a vacancy or insertion in the lattice where a carbon atom is expected such as when a CNT is functionalized. Graphene edges also show up as disorders. The ratio of the intensity of the G band to the D band is used to estimate the quality of the sample grown. The larger the ratio, the higher quality the sample is. The G' band is an indicator of whether a measured sample is CNTs or CNFs. This band is independent of the number of defects in a sample and be used to compare between samples. This value is largest for samples with SWCNT or single layer graphene. The higher this band is, the more 2D structured the sample is. This can be compared with the control samples of CNTs as shown in Figure 4. Figure 15-a shows Raman spectra obtained at different growth temperatures. The sample spectra approach the CF spectra as the temperature increases. This data indicates that CF were grown despite trying to grow CNT. This is due to the size of the catalyst particles produced being too large for CNT growth. CNT and CF have similar growth conditions with the main difference being catalyst size. Figure 15-b shows the average background intensity from  $1400\text{ cm}^{-1}$  to  $1475\text{ cm}^{-1}$ . This background is due to fluorescence in amorphous carbon. The average intensity decreases as temperature increases and shows that amorphous carbon decreases with temperature as well. [59]

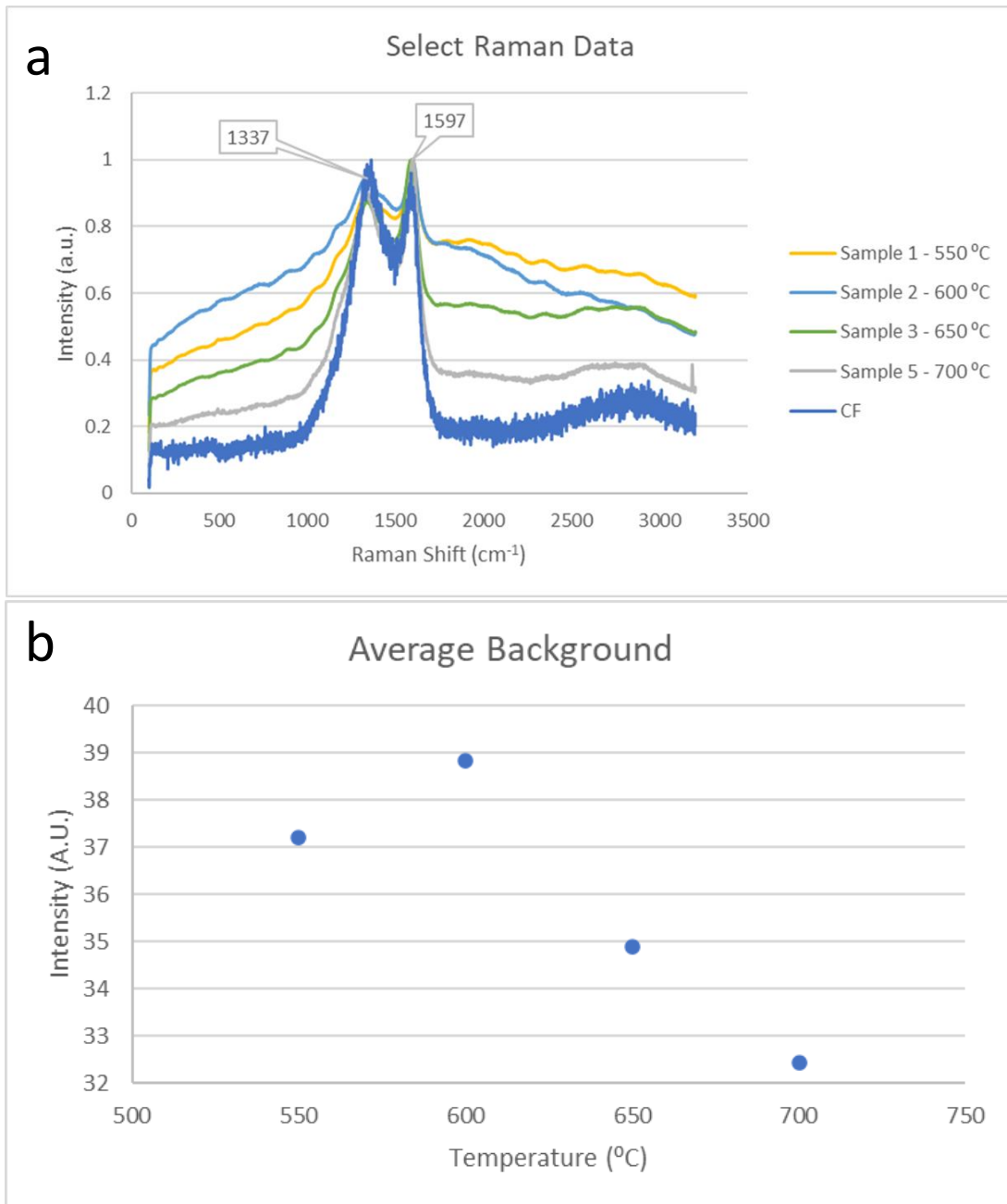


Figure 15: Graph a, average spectra of samples grown at different temperatures. Control sample is CF. Sample spectra approaches CF spectra as temperature increases. Peaks indicate CF was grown. Graph b, average background intensity for each sample from 1400 cm<sup>-1</sup> to 1475 cm<sup>-1</sup>. This background is due to fluorescence within amorphous carbon. This shows a decrease in amorphous carbon as temperature increases. [59]

Raman spectroscopy is not enough on its own to differentiate CNT and graphene. To make the final determination, SEM is used to visualize the sample at 50,000 X, a resolution 50 times greater than that achievable by an optical microscope. SEM can be used to tell the difference between CNT and other forms of carbon. Samples that contain CNTs will have what appear to have long filaments or hairs that may be aligned or randomly oriented. Catalyst particles may be seen along the strands or at the very tips or bases of the tubes. It is very difficult to locate the ends of CNTs as they are only a few nm wide and may be several millimetres to centimetres long. This extreme aspect ratio is a key component of carbon nanotubes. CF appear similar to CNT in SEM but will have a wider diameter.

Figure 16 shows images obtained using SEM. This sample was prepared by pyrolyzing 50 mg of camphor along with 50 mg of zeolite with 5 %wt ferrocene. This sample was held at 600 °C for 15 minutes in an inert argon (Ar) environment. The images show clumps of iron catalyst and the cube-like structure of zeolite. There does not appear to be any CNT or CNF growth. This is likely due to the temperature being too low to allow the ferrocene to efficiently breakdown into proper sized catalyst particles. The temperature may also have been too low to allow for the camphor to pyrolyze and form free carbon radicals, which are the basic building block of CNTs and CNFs. Others were able to successfully grow CNTs at this temperature although they were using a hot wall CVD reactor as opposed to a cold wall reactor. [11] It may be possible to grow CNTs and CNFs with my reactor design at this temperature using a different catalyst material or by varying the catalyst concentration or size. Another method that may allow for successful growth at this temperature is by pre-forming the catalyst particles by heating the zeolite catalyst mixture to a high temperature without a carbon source. This process would allow for the selection of a particle size usually only obtained in a higher temperature run. Photolithography may also be used to deposit metal catalyst particles of a known size at a chosen location and concentration.

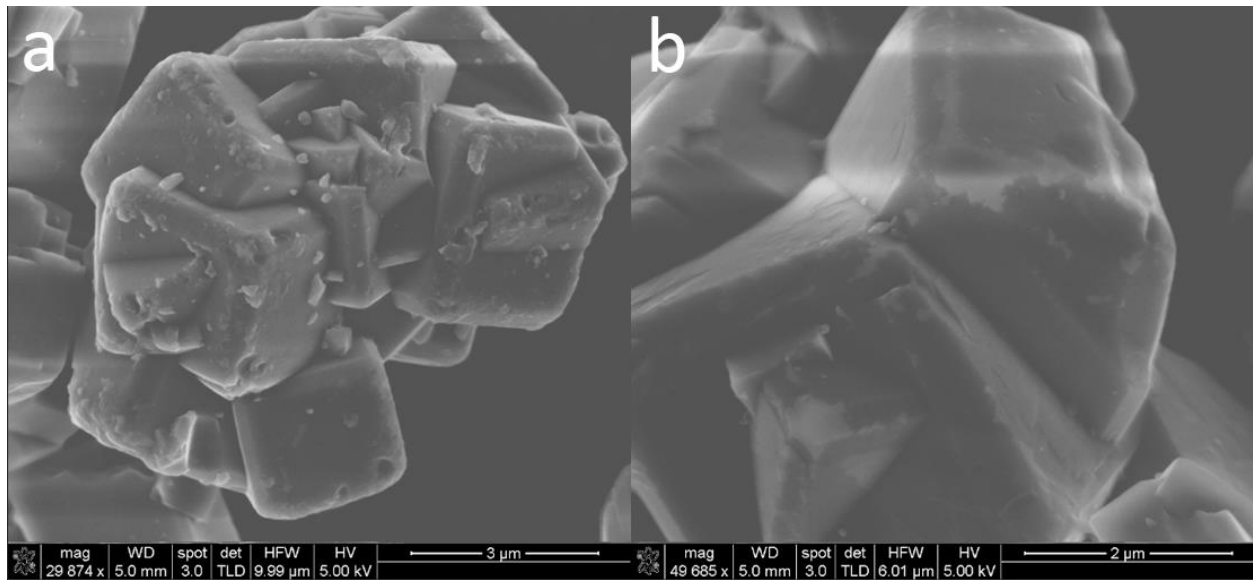


Figure 16: SEM of sample 2 grown at 600 °C. (a) No noticeable CNT or CF growth and (b) very little indication of iron catalyst structures.

Figure 17 shows SEM imaging of a sample grown using 50 mg camphor on 60 mg of zeolite with 5 wt% ferrocene. This sample was grown at 700 °C for 15 minutes in an inert Ar environment. This SEM sample was prepared by sonicating ~ 5 mg of the as grown sample powder in 5 mL of 200 proof ethanol for 15 minutes. The solution was then pipetted onto an aluminium SEM stub and allowed to dry at room temperature for 24 hours. This sample clearly shows long (>10 µm) hair-like filaments. These filaments are likely bundles of CNTs or CNFs that are covered in amorphous carbon. Some of the filaments are likely metal oxide nanowires which grow under similar reaction conditions as CNTs. It is possible that some of the iron in ferrocene contributed to this forming iron oxide nanowires or there may be impurities in the zeolite that caused this. The sample would need to be purified and observed under TEM to confirm this. Image 17-b shows one of the longer filaments in this sample, measured at least 29.4 µm. This appears to be a bundle of several fibre structures that formed together. This is interesting as no other samples that were imaged produced fibres this long. This fibre has a 90° bend and extends beyond the edge of the image. The fibre is likely longer than the measurement result. There also appears to be a network of smaller fibres covering some of the zeolite. This was observed in other samples grown using the same procedure. There are also many small dot-like structures on the zeolite



that are likely iron catalyst nanoparticles. These catalyst particles are responsible for initiating CNT and CNF formation and the diameter of the particles also determines the diameter of any tubes grown. Figure 17-a shows a large bundle of fibre structures one showing a 180° bend, this may be a CNT or a metal oxide nanowire. There is also a structure in Figure 17-d that has the appearance of a ball of yarn. This is possibly the result of the simultaneous growth of many CFs that tangle into a tight ball shape. Other growth methods involve the use of a constant flow of inert gas that may have resulted in the CNTs or CFs being pulled by the gas flow current forming more directionally aligned bundles. Our furnace design has no such force directing the growth and as such the tubes form isotopically and become tangled. These ball structures may also be a zeolite structure that was formed during the growth process. Similar structures were observed in other samples at temperatures as low as 550 °C. This seems to imply they may not be CNTs or CFs, as the lower temperature samples did not have the characteristic fibre structures as those grown at temperatures greater than 700 °C. These tangled ball-like structures may also be metal oxide nanowires, more work is required to determine this.

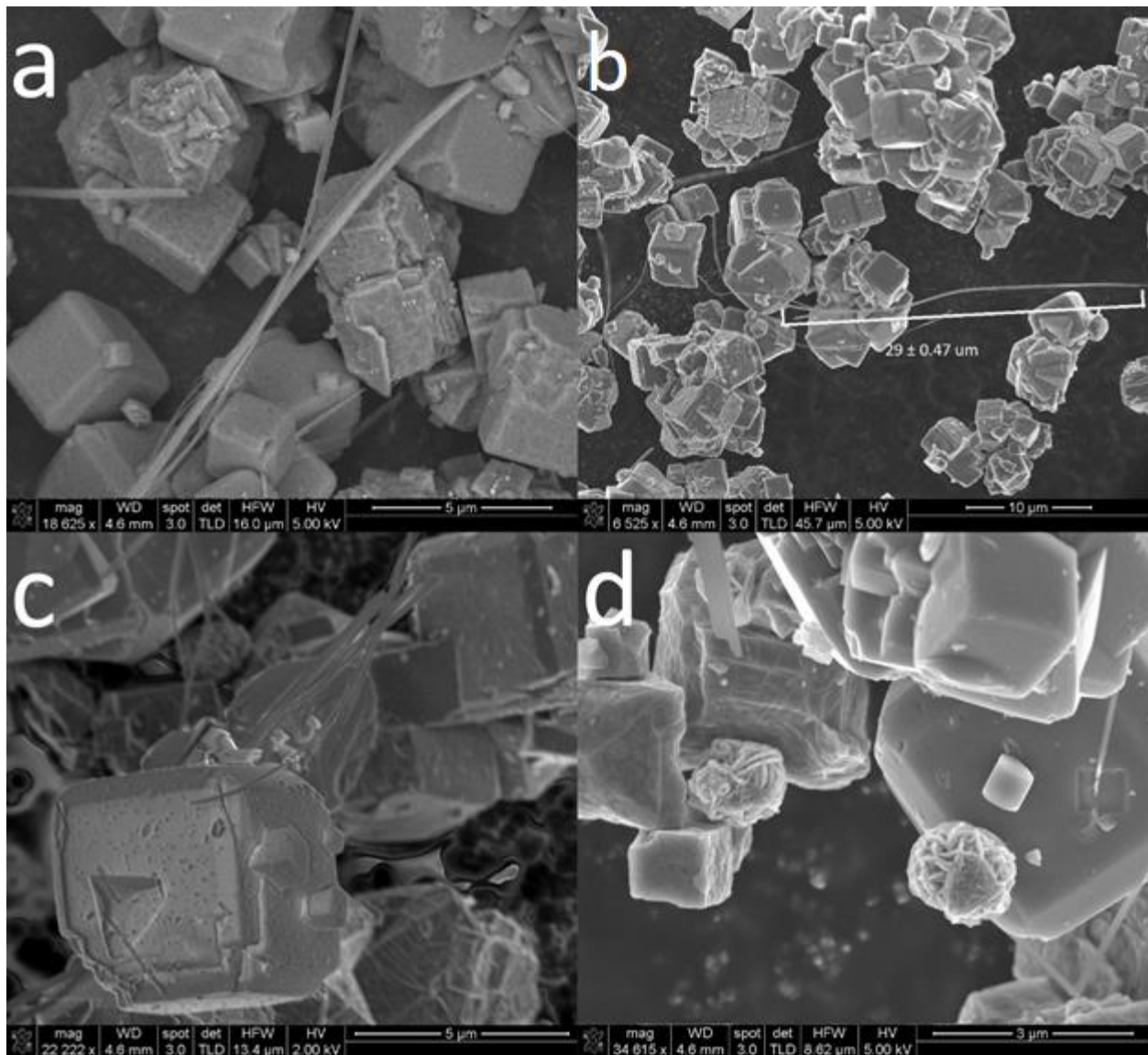


Figure 17: SEM of sample 4, grown at 700 °C. (a) Multiple hair like filaments between zeolite cubes. (b) length of one of the longer fibres, this fibre also exhibits a 90° bend (c) CNTs also appear to be growing on zeolite faces. Small dot structures on surface of zeolite indicative of iron nanoparticle catalyst. (d) Tangled ball-like structures.

Figure 18 shows the SEM imaging of another sample grown under the same conditions as the previous. Post imaging analysis was performed using ImageJ 1.52a software developed by the National Institute of Health. [60] This software was used to measure the diameter of several observed CFs. The measured diameters are greater than 40 nm in diameter, reinforcing that CFs were grown. Image18- c shows a close up of the CF networks that are formed on the surface of

the zeolite particles. There also appears to be a catalyst particle at the end suggesting that this tube grew in the tip-growth fashion. There also appears to be a partially formed ball-like structure with a CF growing out of it. The measured thickness of the CF at 109.9 nm is around the measured diameter of the catalyst particles formed. TEM could be used to determine the structure of the CF as this imaging technique shows a cross-section of the internal structure of the fibre. Image 18-d shows a curled-up CF with a length greater than 1  $\mu\text{m}$ . This fibre appears to have a very constant diameter and again shows the end of the tube where growth terminated. Growth may have been terminated due to catalyst fowling, which occurs when the catalyst particle becomes completely encased in amorphous carbon and no more carbon free radicals are able to reach it. Another reason that growth terminates may be from no more available carbon source to continue the growth reaction. Because my reactor has a fixed amount of camphor that quickly vaporizes, I believe that this caused growth to terminate. I believe that if camphor vapor was constantly refreshed at the substrate then longer fibre growth would result.

A flaw of the reactor design is that the camphor and zeolite are contained in a bell jar with a small volume of 3 mL. When the temperature reached a sufficient point, a thick cloud of camphor and ferrocene vapor quickly forms in the bell jar. As the amount of vapor increases, it begins to exit between the bottom of the inverted bell jar and the quartz plate, coating the cold wall of the quartz tube. As the growth proceeds, the vapor quickly disappears from inside the bell jar. I believe that the escape of camphor vapour limits the amount of available carbon source available in the bell jar and that the tight seal around between the bell jar and the quartz plate prevents the escaped camphor vapour from diffusing back in. This limits the amount of available carbon and thus the length and number of CNTs or CFs grown and observed. This makes it easier to observe the ends of the CFs or CNTs because they are not obscured by other CFs or CNTs as in Figure 6.

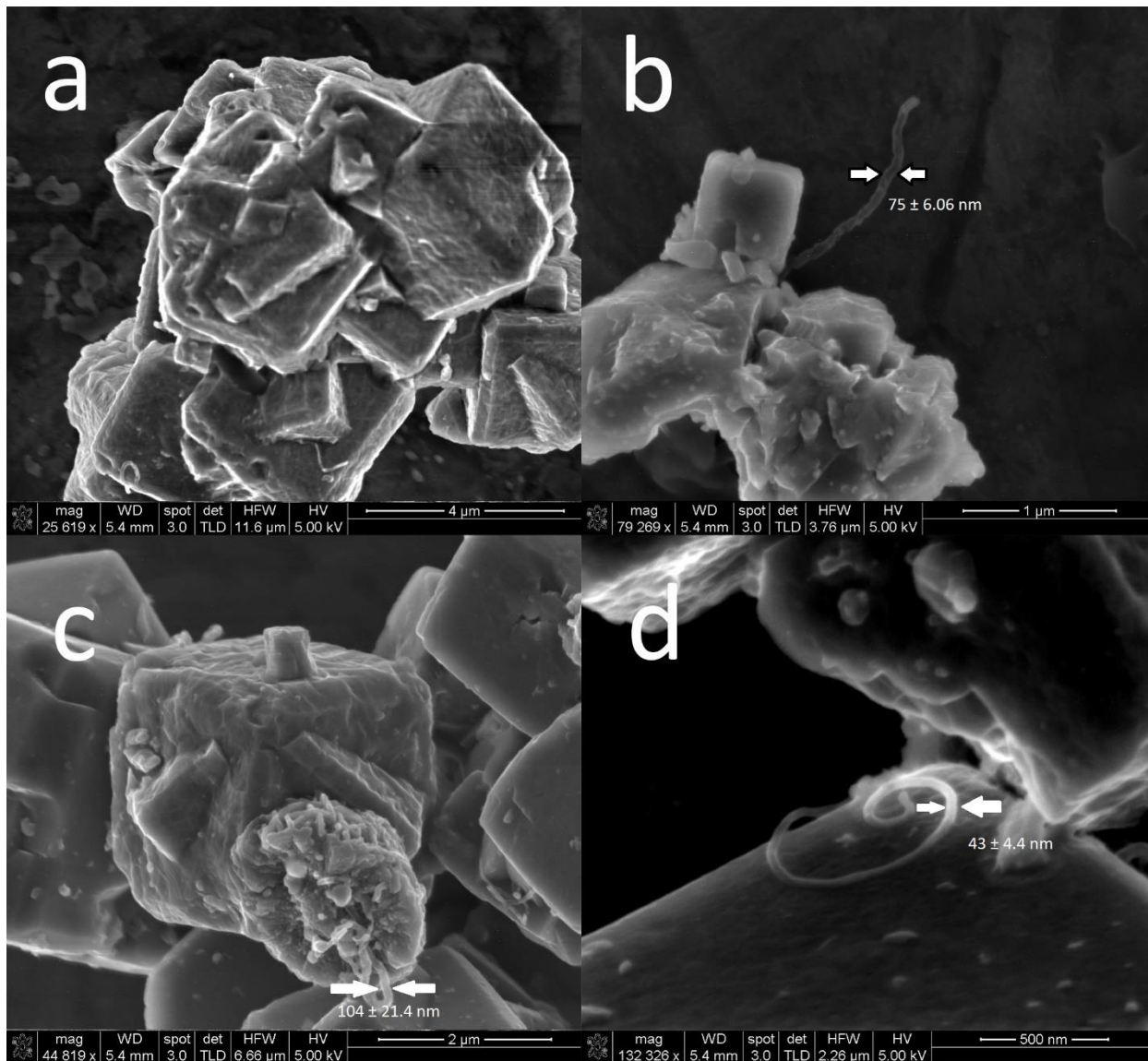


Figure 18: SEM of Sample 7 showing measurement of several different width CFs (a) zeolite faces appear covered in amorphous carbon as well as some tubular structures. (b) width measurement of one of the protruding fibres on the zeolite. (c) measurement of a wider structure on the zeolite. (d) ‘pig-tail’ like structure with width measurement.

Figure 19 shows iron catalyst nanoparticles on the surface of a zeolite cube. Figures 19-b and 19-c shows networks of CNTs or CNFs that formed on the surface. Figure 19-d shows the diameter measurement of several catalyst particles. A more comprehensive statistical analysis was performed using ImageJ (Appendix A, Table 1). Minimum and maximum diameter values were recorded and the mean and standard deviation (SD) were calculated. The average minimum

diameter of the catalyst particles in Figure 19-d was 100 nm. The average maximum diameter and the overall average diameter were 120 nm, and 110 nm, respectively. The SD of the average diameter was 17 nm. These numbers strongly suggest the actual growth of CNF. [17] The Raman spectrum of this sample, located in Figure 15, further indicates that it is CNFs. The lack of a  $G'$  peak around  $2700\text{ cm}^{-1}$  is clearly visible.

figure

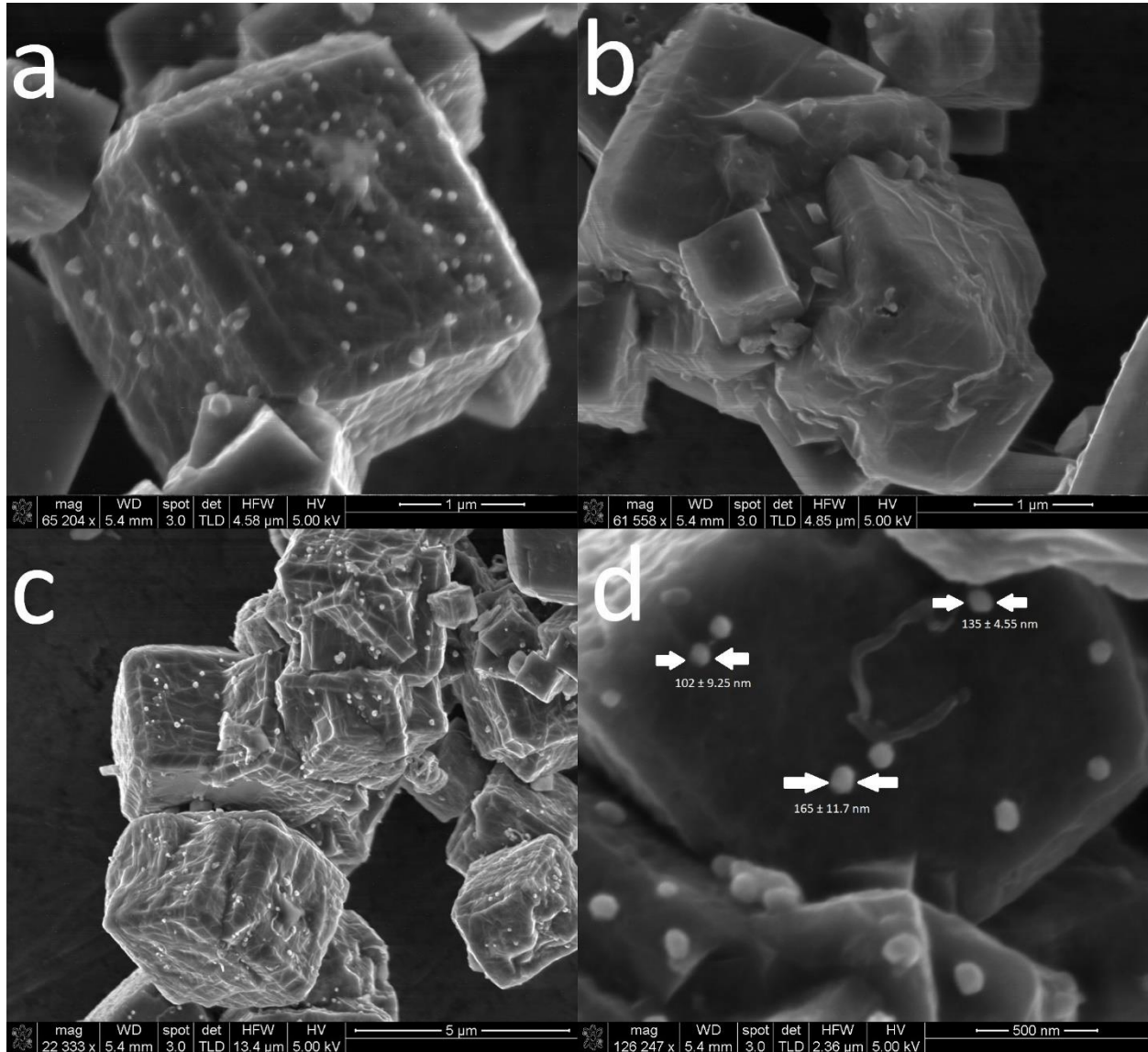


Figure 19: SEM of sample 8 grown at  $700\text{ }^\circ\text{C}$  (a) showing formation of iron catalyst nanoparticles. Image (b) and (c) tubular networks on zeolite surface. (d) catalyst width measurements with error range.

## Chapter 4: Conclusions and Future Work

### 4.1 Conclusion and Discussion

This work presented herein demonstrates the construction and use of a cold wall CVD reactor for the production of CNFs from camphor. More work is required to confirm the presence of CNTs. This reactor design is easily constructed and inexpensive. The reactor consists of a high temperature ceramic heater that is used to heat a quartz plate on top of which the carbon source and catalyst materials are placed. A thermocouple is placed in the centre of the bottom surface of the ceramic heater and this assembly is tied together with wire and inserted into a 50 mm O.D. quartz tube. The thermocouple is used to control the reaction temperature via a PID controller that cycles power to the ceramic heater.

The effect of reaction temperature was observed using Raman spectroscopy and SEM. Reaction temperature was varied from 550 °C to 750 °C. The tube was flushed with argon to create an inert environment. Reaction time was held constant at 15 minutes. Ferrocene concentration was held constant at 5 wt% with zeolite. Every reaction was run with 50 mg of camphor and 50 mg of zeolite.

No fibres were observed in the samples grown at 550 °C and 600 °C. At 650 °C limited fibre growth was observed. At temperatures above 700 °C much more fibre growth was observed as well as well-defined catalyst particles. Further work is necessary to optimize this reactor for the growth of CNTs at a significant yield. The observed fibre structures may be CNFs as indicated by their Raman spectra as well as the diameter of the catalyst particles and fibres. A lower concentration of ferrocene would likely favour the formation of smaller iron particles. The diameter of the grown CNTs and CNFs is highly dependent on catalyst size with smaller catalyst particles favouring CNTs.

The samples used here contain large amounts of amorphous carbon, zeolite, and iron nanoparticles. For future study, it would be ideal to separate the grown carbon nanomaterials from the zeolite and remove as much amorphous carbon and iron from the sample as possible.

To remove the amorphous carbon and any spherical carbon in the sample, oxidation is the most widely used method. Chlorine gas could be used to oxidize the amorphous carbon from the sample.[61] The zeolite could be removed by suspending the nanotube and zeolite mixture in solution and using a centrifuge to pull the denser zeolite to the bottom.

A possible source of contamination is the cleaning procedure used to prepare samples for SEM observation. The cleaning procedure mentioned on page 29 likely results in large amounts of residue. A triple cleaning process like used in the electronics fabrication industry would be better. This process is derived from the triple clean used in electronics fabrication to clean silicon wafers. Solvents remove organic residues from the sample but also leave a residue themselves. A triple clean can be performed to help minimize contamination. This process involves using solvents such deionized water, acetone, and methanol. First the sample is soaked in warm (< 55 °C) acetone for 5 minutes. The sample is then removed by filtration and soaked in a room temperature methanol bath for 2-5 minutes. The sample is again removed by filtration. The filtrate is then rinsed with deionized water and dried for 24 hours.

Carbon nanofibers can be made from a solid carbon source, which is proven by using camphor as a case study material. A possible alteration to the experimental setup would be to add a glass tube that feeds into the quartz bell jar to constantly supply camphor vapour from an external heater, or the bell jar could be removed with a constant flow of camphor being carried to the substrate by an inert carrier gas. Further work could be done to determine optimal reaction conditions.

Appendix A: Supplementary Data

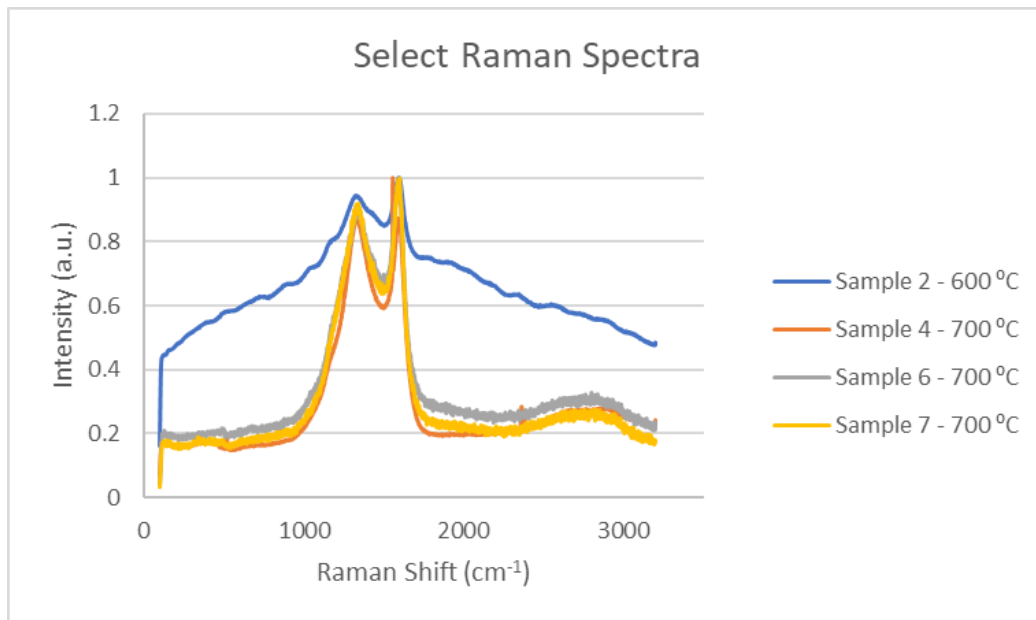


Figure 20 Raman spectra of three samples grown at 700 °C and one at 600 °C



Sample #	Page#	Temperature °C
1	BK1P36	550
2	BK1P37	600
3	BK1P38	650
4	BK1P45	700
5	BK1P49	700
6	BK1P58	700
7	BK1P60	700
8	BK1P62	700

*Figure 21 sample number to lab book correlation*

## Glossary

Amorphous carbon – free carbon that does not have any crystalline structure

Ballistic transport – transport of a charge carrier through a medium with negligible resistivity due to scattering

Camphor – waxy, aromatic terpene from the camphor laurel

Carbon fibre – carbon structure with diameter greater than 50 nm with consisting of stacked layers of graphene

Carbon nanotube – very high aspect ratio carbon structure consisting of one or more layers of graphene rolled into a hollow tube. Diameter is typically less than 50 nm

Catalyst – a substance that increases the rate of a chemical reaction without undergoing change

Catenation – the bonding of atoms of the same element into repeating chain

Chemical vapour deposition – synthesis technique that involves the introduction of a precursor in a gas state to interact with a surface

Chirality – measure of angle between nanotube axis and carbon chain direction. Determines many properties of the CNT such as resistivity

Energy Dispersive X-Ray Spectroscopy – spectrographic technique that uses the interaction of X-rays with the atoms of a specimen used to determine elemental composition

Graphene – planar sheet of  $sp^2$  bonded carbon forming a network of hexagonal bonds

Liquid injection reactor – CVD reactor that introduces precursors in a liquid form via continuous feed

NiCr wire – nickel chromium wire with high electrical resistivity used as a heating element

PID controller – programable temperature controller that compensates for overshoot and power fluctuations by varying the power cycle of a heater using a thermocouple to measure the current temperature of the heating element

Raman Spectroscopy – spectroscopic technique that uses the interaction of light with chemical bonds in a sample to generate higher energy photons that are used to generate a molecular fingerprint of a material.

Scanning Electron Microscopy – microscopy technique that uses an electron beam to scan the surface of a material by measuring reflected and scattered electrons. Generates a high detail image of a samples surface with nanometre resolution

Thermocouple – temperature sensor consisting of the junction of two dissimilar metals. A voltage is created at the junction that varies in proportion to temperature and is used to determine temperature

Transmission Electron Microscopy – microscopy technique that uses electrons to image a very thin sample. Gives cross sectional detail of structures such as CNTs

Andrew Anderson

Van der Waals – weak force that attracts molecules to one another. This is the force between layers of graphene in graphite as well as CNFs.

## References

- [1] Kroto, H. W.; Heath, J. R.; O'Brien, S. C.; Curl, R. F.; Smalley, R. E. C60: Buckminsterfullerene. *Nature* **1985**, *318*, 162–163.
- [2] Neto, A. H. C.; Guinea, F.; Peres, N. M. R.; Novoselov, K. S.; Geim, A. K. The Electronic Properties of Graphene. *Reviews of Modern Physics* **2009**, *81*, 109–162.
- [3] Novoselov, K. S. Electric Field Effect in Atomically Thin Carbon Films. *Science* **2004**, *306*, 666–669.
- [4] Lee, C.; Wei, X.; Kysar, J. W.; Hone, J. Measurement of the Elastic Properties and Intrinsic Strength of Monolayer Graphene. *Science* **2008**, *321*, 385–388.
- [5] Allen, M. J.; Tung, V. C.; Kaner, R. B. Honeycomb Carbon: A Review of Graphene. *Chemical Reviews* **2010**, *110*, 132–145.
- [6] Hernaez, M.; Zamarreño, C.; Melendi-Espina, S.; Bird, L.; Mayes, A.; Arregui, F. Optical Fibre Sensors Using Graphene-Based Materials: A Review. *Sensors* **2017**, *17*, 155.
- [7] Jo, J. Y.; Kim, B. G. Carbon Allotropes with Triple Bond Predicted by First-Principle Calculation: Triple Bond Modified Diamond AndT-Carbon. *Physical Review B* **2012**, *86*.
- [8] Kim, B. G.; Sim, H.; Park, J. C4 Carbon Allotropes with Triple-Bonds Predicted by First-Principles Calculations. *Solid State Communications* **2013**, *169*, 50–56.
- [9] Zhang, R.; Zhang, Y.; Zhang, Q.; Xie, H.; Qian, W.; Wei, F. Growth of Half-Meter Long Carbon Nanotubes Based on Schulz–Flory Distribution. *ACS Nano* **2013**, *7*, 6156–6161.
- [10] Dresselhaus, M.; Dresselhaus, G.; Saito, R.; Jorio, A. Raman Spectroscopy of Carbon Nanotubes. *Physics Reports* **2005**, *409*, 47–99.
- [11] Kumar, M.; Ando, Y. A Simple Method of Producing Aligned Carbon Nanotubes from an Unconventional Precursor – Camphor. *Chemical Physics Letters* **2003**, *374*, 521–526.
- [12] Keskar, G.; Rao, R.; Luo, J.; Hudson, J.; Chen, J.; Rao, A. M. Growth, Nitrogen Doping and Characterization of Isolated Single-Wall Carbon Nanotubes Using Liquid Precursors. *Chemical Physics Letters* **2005**, *412*, 269–273.
- [13] Hiremath, N.; Bhat, G. High-Performance Carbon Nanofibers and Nanotubes. *Structure and Properties of High-Performance Fibers* **2017**, 79–109.
- [14] Balasubramanian, K.; Burghard, M. Chemically Functionalized Carbon Nanotubes. *Small* **2005**, *1*, 180–192.

- [15] Vera-Agullo, J.; Varela-Rizo, H.; Conesa, J. A.; Almansa, C.; Merino, C.; Martin-Gullon, I. Evidence for Growth Mechanism and Helix-Spiral Cone Structure of Stacked-Cup Carbon Nanofibers. *Carbon* **2007**, *45*, 2751–2758.
- [16] Liu, B.; Ren, W.; Gao, L.; Li, S.; Pei, S.; Liu, C.; Jiang, C.; Cheng, H.-M. Metal-Catalyst-Free Growth of Single-Walled Carbon Nanotubes. *Journal of the American Chemical Society* **2009**, *131*, 2082–2083.
- [17] Jong, K. P. D.; Geus, J. W. Carbon Nanofibers: Catalytic Synthesis and Applications. *Catalysis Reviews* **2000**, *42*, 481–510.
- [18] Cheung, C. L.; Kurtz, A.; Park, H.; Lieber, C. M. Diameter-Controlled Synthesis of Carbon Nanotubes. *The Journal of Physical Chemistry B* **2002**, *106*, 2429–2433.
- [19] Chhowalla, M.; Teo, K. B.; Ducati, C.; Rupesinghe, N. L.; Amaratunga, G. A.; Ferrari, A. C.; Roy, D.; Robertson, J.; Milne, W. I. Growth Process Conditions of Vertically Aligned Carbon Nanotubes Using Plasma Enhanced Chemical Vapor Deposition. *Journal of Applied Physics* **2001**, *90*, 5308–5317.
- [20] Terrones, M. Science and Technology of the Twenty-First Century: Synthesis, Properties, and Applications of Carbon Nanotubes. *Annual Review of Materials Research* **2003**, *33*, 419–501.
- [21] Welna, D. T.; Qu, L.; Taylor, B. E.; Dai, L.; Durstock, M. F. Vertically Aligned Carbon Nanotube Electrodes for Lithium-Ion Batteries. *Journal of Power Sources* **2011**, *196*, 1455–1460.
- [22] Sanginario, A.; Miccoli, B.; Demarchi, D. Carbon Nanotubes as an Effective Opportunity for Cancer Diagnosis and Treatment. *Biosensors* **2017**, *7*, 9.
- [23] Andreoli, E.; Barron, A. R. Correlating Carbon Dioxide Capture and Chemical Changes in Pyrolyzed Polyethylenimine-C60. *Energy & Fuels* **2015**, *29*, 4479–4487.
- [24] Serda, M.; Ware, M. J.; Newton, J. M.; Sachdeva, S.; Krzykawska-Serda, M.; Nguyen, L.; Law, J.; Anderson, A. O.; Curley, S. A.; Wilson, L. J.; *et al.* Development of Photoactive Sweet-C60 for Pancreatic Cancer Stellate Cell Therapy. *Nanomedicine* **2018**, *13*, 2981–2993.
- [25] Lu, W.; Zu, M.; Byun, J.-H.; Kim, B.-S.; Chou, T.-W. State of the Art of Carbon Nanotube Fibers: Opportunities and Challenges. *Advanced Materials* **2012**, *24*, 1805–1833.
- [26] Dresselhaus, M.; Dresselhaus, G.; Saito, R. Physics of Carbon Nanotubes. *Carbon Nanotubes* **1996**, 27–35.
- [27] Lau, A. K.-T.; Hui, D. The Revolutionary Creation of New Advanced Materials—Carbon Nanotube Composites. *Composites Part B: Engineering* **2002**, *33*, 263–277.
- [28] Dai, H.; Javey, A.; Pop, E.; Mann, D.; Kim, W.; Lu, Y. Electrical Transport Properties And Field Effect Transistors Of Carbon Nanotubes. *Nano* **2006**, *01*, 1–13.

- [29] Ando, T.; Matsumura, H.; Nakanishi, T. Theory of Ballistic Transport in Carbon Nanotubes. *Physica B: Condensed Matter* **2002**, *323*, 44–50.
- [30] Kumanek, B.; Janas, D. Thermal Conductivity of Carbon Nanotube Networks: a Review. *Journal of Materials Science* **2019**, *54*, 7397–7427.
- [31] Cedillos-Barraza, O.; Manara, D.; Boboridis, K.; Watkins, T.; Grasso, S.; Jayaseelan, D. D.; Konings, R. J. M.; Reece, M. J.; Lee, W. E. Investigating the Highest Melting Temperature Materials: A Laser Melting Study of the TaC-HfC System. *Scientific Reports* **2016**, *6*.
- [32] Cambridge University Engineering Department (**2003**). Materials Data Book. Cambridge.
- [33] Bai, Y.; Zhang, R.; Ye, X.; Zhu, Z.; Xie, H.; Shen, B.; Cai, D.; Liu, B.; Zhang, C.; Jia, Z.; *et al.* Carbon Nanotube Bundles with Tensile Strength over 80 GPa. *Nature Nanotechnology* **2018**, *13*, 589–595.
- [34] Lalwani, G.; Henslee, A. M.; Farshid, B.; Lin, L.; Kasper, F. K.; Qin, Y.-X.; Mikos, A. G.; Sitharaman, B. Two-Dimensional Nanostructure-Reinforced Biodegradable Polymeric NANOCOMPOSITES for Bone Tissue Engineering. *Biomacromolecules* **2013**, *14*, 900–909.
- [35] Volder, M. F. L. D.; Tawfick, S. H.; Baughman, R. H.; Hart, A. J. Carbon Nanotubes: Present and Future Commercial Applications. *Science* **2013**, *339*, 535–539.
- [36] Chen, P.; Fu, Y.; Aminirad, R.; Wang, C.; Zhang, J.; Wang, K.; Galatsis, K.; Zhou, C. Fully Printed Separated Carbon Nanotube Thin Film Transistor Circuits and Its Application in Organic Light Emitting Diode Control. *Nano Letters* **2011**, *11*, 5301–5308.
- [37] Chai, Y.; Chan, P. C. High Electromigration-Resistant Copper/Carbon Nanotube Composite for Interconnect Application. *2008 IEEE International Electron Devices Meeting* **2008**.
- [38] Oberlin, A.; Endo, M.; Koyama, T. Filamentous Growth of Carbon through Benzene Decomposition. *Journal of Crystal Growth* **1976**, *32*, 335–349.
- [39] Eatemadi, A.; Daraee, H.; Karimkhanloo, H.; Kouhi, M.; Zarghami, N.; Akbarzadeh, A.; Abasi, M.; Hanifehpour, Y.; Joo, S. Carbon Nanotubes: Properties, Synthesis, Purification, and Medical Applications. *Nanoscale Research Letters* **2014**, *9*, 393.
- [40] Iijima, S. Helical Microtubules of Graphitic Carbon. *Nature* **1991**, *354*, 56–58.
- [41] Guo, T.; Nikolaev, P.; Rinzler, A. G.; Tomanek, D.; Colbert, D. T.; Smalley, R. E. Self-Assembly of Tubular Fullerenes. *The Journal of Physical Chemistry* **1995**, *99*, 10694–10697.
- [42] Chrzanowska, J.; Hoffman, J.; Małolepszy, A.; Mazurkiewicz, M.; Kowalewski, T. A.; Szymanski, Z.; Stobinski, L. Synthesis of Carbon Nanotubes by the Laser Ablation Method: Effect of Laser Wavelength. *physica status solidi (b)* **2015**, *252*, 1860–1867[43] Cantoro, M.; Hofmann, S.; Pisana, S.; Scardaci, V.; Parvez, A.; Ducati, C.; Ferrari, A. C.; Blackburn, A. M.; Wang, K.-Y.;

Robertson, J. Catalytic Chemical Vapor Deposition of Single-Wall Carbon Nanotubes at Low Temperatures. *Nano Letters* **2006**, *6*, 1107–1112.

[44] Lee, Y. D.; Lee, H. J.; Han, J. H.; Yoo, J. E.; Lee, Y.-H.; Kim, J. K.; Nahm, S.; Ju, B.-K. Synthesis of Double-Walled Carbon Nanotubes by Catalytic Chemical Vapor Deposition and Their Field Emission Properties. *The Journal of Physical Chemistry B* **2006**, *110*, 5310–5314.

[45] Kunadian, I.; Andrews, R.; Qian, D.; Mengüç, M. P. Growth Kinetics of MWCNTs Synthesized by a Continuous-Feed CVD Method. *Carbon* **2009**, *47*, 384–395.

[46] Manawi, Y.; Ihsanullah; Samara, A.; Al-Ansari, T.; Atieh, M. A Review of Carbon Nanomaterials' Synthesis via the Chemical Vapor Deposition (CVD) Method. *Materials* **2018**, *11*, 822.

[47] Teo, K. B. K.; Chhowalla, M.; Amaratunga, G. A. J.; Milne, W. I.; Hasko, D. G.; Pirio, G.; Legagneux, P.; Wyczisk, F.; Pribat, D. Uniform Patterned Growth of Carbon Nanotubes without Surface Carbon. *Applied Physics Letters* **2001**, *79*, 1534–1536.

[48] Zhang, W.; Wen, Y.; Tjiu, W.; Xu, G.; Gan, L. Growth of Vertically Aligned Carbon-Nanotube Array on Large Area of Quartz Plates by Chemical Vapor Deposition. *Applied Physics A: Materials Science & Processing* **2002**, *74*, 419–422.

[49] Feng, J.-M.; Wang, R.; Li, Y.-L.; Zhong, X.-H.; Cui, L.; Guo, Q.-J.; Hou, F. One-Step Fabrication of High Quality Double-Walled Carbon Nanotube Thin Films by a Chemical Vapor Deposition Process. *Carbon* **2010**, *48*, 3817–3824.

[50] Ravani, F.; Papagelis, K.; Dracopoulos, V.; Parthenios, J.; Dassios, K. G.; Siokou, A.; Galiotis, C. Graphene Production by Dissociation of Camphor Molecules on Nickel Substrate. *Thin Solid Films* **2013**, *527*, 31–37.

[51] Eba, R. Characterization of Carbon Nanotubes. *Physical and Chemical Properties of Carbon Nanotubes* **2013**.

[52] Chattopadhyay, D.; Galeska, I.; Papadimitrakopoulos, F. Complete Elimination of Metal Catalysts from Single Wall Carbon Nanotubes. *Carbon* **2002**, *40*, 985–988.

[53] Miyata, Y.; Mizuno, K.; Kataura, H. Purity and Defect Characterization of Single-Wall Carbon Nanotubes Using Raman Spectroscopy. *Journal of Nanomaterials* **2010**, *2011*, 1–7.

[54] Pecl, G. T.; Araújo, M. B.; Bell, J. D.; Blanchard, J.; Bonebrake, T. C.; Chen, I.-C.; Clark, T. D.; Colwell, R. K.; Danielsen, F.; Evengård, B.; et al. Biodiversity Redistribution under Climate Change: Impacts on Ecosystems and Human Well-Being. *Science* **2017**, 355.

[55] Zuccarini, P. Camphor: Risks and Benefits of a Widely Used Natural Product. *Journal of Applied Sciences and Environmental Management* **2010**, *13*.

Andrew Anderson

[62] Yu, M. Strength and Breaking Mechanism of Multiwalled Carbon Nanotubes Under Tensile Load. *Science* **2000**, *287*, 637–640.

[63] Pavan M. V. Raja, Andrew R. Barron, *Physical Methods in Chemistry and Nano Science*. OpenStax CNX. Jan 20, **2019**